Asia-Pac. J. Atmos. Sci., 53(1), 101-120, 2017
DOI:10.1007/s13143-017-0009-4

pISSN 1976-7633 / eISSN 1976-7951

Physical and Dynamic Factors That Drove the Heavy Rainfall Event Over the middle Korean Peninsula on 26-27 July 2011

Joo-Young Lee, Wonsu Kim, and Tae-Young Lee

Department of Atmospheric Sciences and Global Environment Laboratory, Yonsei University, Seoul, Korea

(Manuscript received 23 March 2016; accepted 19 October 2016)

Abstract: This study used an observational analysis and a numerical model to investigate the heavy rainfall event that occurred on 26-27 July 2011 over the middle Korean Peninsula. Radar observations revealed a significant transition in the echo pattern, with strong convective systems along the coasts of southern Hwanghae-do (HHD) and Gyeonggi-do (0600-1200 UTC 26 July, stage 1), a medium-sized SW-NE precipitation band over the middle Korean Peninsula and major convective systems in the west (1500-2200 UTC, stage 2), and a narrow convective band from Gyeonggi Bay to the Seoul metropolitan area (2200 UTC 26-0100 UTC 27 July, stage 3). This study focused on the development of heavy precipitation systems during stages 1 and 2. A mesoscale ridge and trough developed over the middle peninsula at approximately 0600 UTC on 26 July and persisted throughout the first 2 stages. Both the observation and the numerical simulation suggest that a cold pool, which induced the mesoscale ridge, developed over the inland HHD in response to evaporative cooling of rain water. The outflow associated with the cold pool was found to trigger the strong convective systems along the southern coast of HHD in stage 1. The lifting of air in the precipitation band of stage 2 was mainly caused by convergence ahead of the strong low-level southwesterly flow. The numerical simulations indicated that the terrain over the Korean Peninsula contributed to the enhancement of the heavy rainfall primarily through its blocking effects on oncoming southwesterly airflow at low levels.

Key words: Heavy precipitation systems, mesoscale ridge, evaporative cooling, terrain effect

1. Introduction

Relatively long-lasting heavy rainfall occurred over the middle Korean Peninsula on 26-28 July 2011, and particularly large amounts of rain exceeding 300 mm were recorded in Seoul and central Gyeonggi-do (GGD) during the first day (i.e., 0000 UTC 26-0000 UTC 27 July) (Fig. 1). The heavy rainfall resulted in considerable losses of life and property, especially in Seoul (NEMA, 2012).

Because of the intensity of the heavy rainfall and the magnitude of the resulting losses, this heavy rainfall event has attracted attention from experts in various fields related to natural disasters, including meteorology. Additionally, various meteorological analyses have been used to explain the event. Lee et al. (2014a) studied the environmental conditions and structure of a band-type precipitation system over a 4-h period on the morning of 27 July 2011 (i.e., 2100 UTC 26 July-0100 UTC 27 July, where LST = UTC + 9 h) using various observational data. The authors found that thermodynamic instability and the presence of a trough over the Korean Peninsula favored the development of the precipitation system. Analyses by operational weather forecasters of the Korea Meteorological Administration (KMA) suggested that a stationary pressure system, a low-level jet, and thermodynamic instability were the major contributors to the development of the heavy rainfall event (KMA, 2012).

Heavy precipitation systems (HPSs) over the Korean Peninsula during the summer are closely associated with the general synoptic-scale environment (Hong, 2004; Lee et al., 2008). The role of the large-scale environment is particularly important for long-lasting heavy rainfall events. Lee et al. (2008) studied the synoptic-scale environment associated with

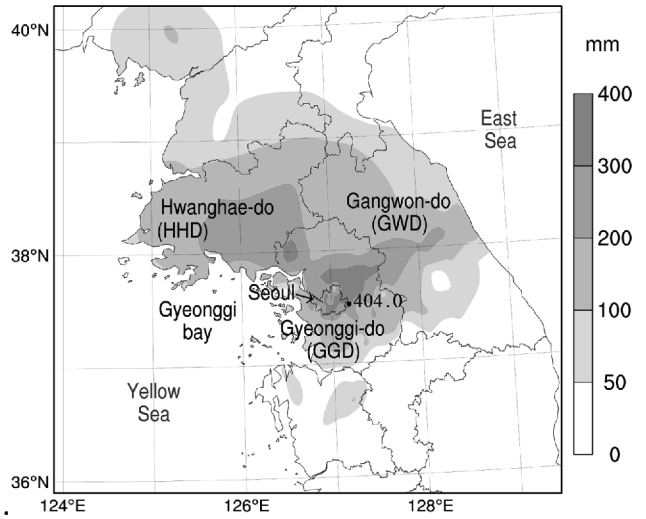

Fig. 1. Accumulated rainfall amounts (mm) from the measurements at synoptic weather stations and automatic weather stations (AWSs) for 0000 UTC 26 July-0000 UTC 27 July 2011. A dot indicates the location of the AWS station where the maximum rainfall amount of 404.0 mm was recorded.

Corresponding Author: Wonsu Kim, Department of Atmospheric Sciences, Yonsei University, 50 Yonsei-ro, Seodaemun-gu, Seoul 03722, Korea.
E-mail: wonsukim@yonsei.ac.kr

heavy rainfall events that lasted for 18 days over the summer of 1998. The authors noted that an elongated monsoonal front was maintained over central China and throughout the Korean Peninsula for 20 days, and strong summertime baroclinicity developed between the continental polar low over the north of Korea and the northwestern Pacific high. The quasi-stationary locations of the upper- and low-level jets were important for the heavy rainfall events. For heavy rainfall in which band-type HPSs persisted for approximately 18 hours, Shin and Lee (2005) found that a favorable large-scale environment and its interaction with convective systems might have been important.

The initiation of mesoscale convective systems (MCSs) is a subject of considerable interest. The initiation of MCSs often occurs in association with surface fronts (Bluestein and Jain, 1985; Kato, 1998). The convergence associated with a meso-scale depression and a low-level jet is also an important initiation mechanism for MCS development along the Baiu-Changma-Meiyu fronts (Lee et al., 1998a; Yamada et al., 2003; Choi et al., 2011; Zhang et al., 2014). Mesoscale convective systems may also be triggered along outflow boundaries associated with cold pools (Kim and Lee, 2006; Tsuguti and Kato, 2014; Jeong et al., 2016).

Mountainous terrain can play an important role in the development of heavy rainfall, both directly and indirectly (Chen et al., 1991; Yoshizaki et al., 2000; Kim and Lee, 2006). Kim and Lee (2006) stated that the concentration of convective cells on the western side of the Taebaek Mountain range might be caused by terrain-induced storm obstructions. Terrain effects on heavy rainfall over South Korea are primarily caused by the topography in the middle and southern Korean Peninsula (Lim and Lee, 1994; Seo and Lee, 1996; Kim and Chun, 2000; Lee et al., 2014b). The northern Korean mountain complex (KMC) is known to significantly affect the incoming air flow from the north in winter (e.g., Nagata, 1991; Lee et al., 1998b) and promote heavy snowfall over the east coast of the middle Korean Peninsula (Lee and Park, 1996; Lee and Kim, 2009). The KMC consists of the Gaema Plateau and the surrounding major mountain ranges in the northern Korean Peninsula. The effects of KMC on the development of heavy rainfall in the middle Korean Peninsula have not yet been reported.

The heavy rainfall event over the middle Korean Peninsula during 0000 UTC 26-0000 UTC 27 July 2011 can be of significant interest in terms of physical and dynamical factors that drive the HPS development during the event, in which significant transitions of precipitation-system pattern are noticed by radar observation. The transitions may indicate the possibility of change in the factors that drive the HPS development. The event will be divided into three stages based on echo pattern in the following section. As already mentioned, previous studies on this heavy rainfall event have mostly focused on the 4-h period of 2100 UTC 26-0100 UTC 27 July 2011 (which may belong to stage 3), in which a narrow convective band produced a very intense rainfall. However, no study has been reported on the heavy rainfall during the previous 18 hours (i.e., 0300 UTC-2100 UTC 26 July; stages 1 and 2), in which HPSs continuously developed and produced large amount of rainfall exceeding 200 mm over much of the west-middle Korean Peninsula. The present study is concerned with the heavy rainfall in this 18-h period. Section 2 presents an observational analysis of the precipitation systems and atmospheric structure associated with the development of heavy rainfall. Section 3 presents an analysis of the numerical simulation and a discussion of the physical and dynamic factors for the development of the present HPSs. Section 4 provides a summary and the study conclusions.

2. Observational analysis

An observational analysis of this heavy rainfall event was conducted using synoptic weather station and automatic weather station (AWS) data, rawinsonde data, Communication, Ocean and Meteorological Satellite (COMS) images (http://nmsc.kma.go.kr/html/homepage/en/main.do), composite weather radar constant-altitude plan position indicator (CAPPI) images, and initialized data (12-km grid data) from the Regional Data Assimilation and Prediction System (RDAPS) of the KMA. RDAPS is based on Unified Model (UM) from UK Met Office and initialized by the four-dimensional variational data assimilation system (http://web.kma.go.kr/eng/biz/forecast_02.jsp).

a. Synoptic and mesoscale environment

Surface and 500-hPa charts for 0000 UTC on 26 and 27 July 2011 are presented in Fig. 2. The sea-level pressure (SLP) patterns show a large-scale high-pressure system and a continental low-pressure system to the east and west of the Korean Peninsula, respectively (Figs. 2a and 2b). The stationary western Pacific subtropical high (WPSH) and the ridge over the Sakhalin Islands extending from the WPSH blocked the eastward movement of the low-pressure systems. As a result, a relatively strong W-E-oriented pressure gradient was maintained at a low level along the Yellow Sea (YS) and the Korean Peninsula in the SSW-NNE and SW-NE directions. This pressure pattern produced low-level southerly to southwesterly winds over the YS and the west coast of the Korean Peninsula. The 500-hPa chart also indicates a blocking high and a stagnant trough over the Sakhalin Islands and the continent, respectively (Figs. 2c and 2d). Thus, the heavy rainfall event under consideration occurred between a stagnant high-pressure system and a continental low to the east and west of the Korean Peninsula, respectively. Analysis using RDAPS data indicates that synoptic-scale environment was favorable for the development of HPSs providing ascent of air around the Korean Peninsula through warm air advection (Fig. 2). Vorticity advection at 500 hPa was not significant around the peninsula (not shown). The vertical motion shown in Figs. 2c and 2d may also contain convective ascent.

The geopotential height, the equivalent potential temperature (θ_e) and the winds at 925 hPa are shown in Fig. 3 at 6-h interval. At 0600 UTC 26 July, height contours were aligned in

the SSW-NNE direction and a relatively strong SSW flow occurred from the southern YS to the west coast of the middle Korean Peninsula (Fig. 3a). High-θ_e air (i.e., $\theta_e > 355$ K) was transported from the East China Sea to the west coast by the strong SSW flow. A mesoscale ridge extended northwestward from the Wonsan area (marked by "Δ" in Fig. 3b). These features were still present at 1200 UTC (Fig. 3b). Certain noticeable changes in the heights and the winds occurred after 1200 UTC over much of the Korean Peninsula. The direction of height contours over the southern Korean Peninsula turned toward the northeast as a mesoscale trough developed on the east coast of the middle Korean Peninsula at 1800 UTC (Fig. 3c), and an area with a weak height gradient was identified across the middle Korean Peninsula up to Wonsan. Winds over the southern YS strengthened in a southwesterly direction and moved toward the middle Korean Peninsula. As a result of the weak height gradient, the southwesterly wind rapidly weakened over the inland area of the middle Korean Peninsula. A similar weakening of the wind over the same area was not found at or above 850 hPa (not shown). At 0000 UTC 27 July, a weak height gradient was still present over the middle and northern Korean Peninsula (Fig. 3d). The southwesterly winds rapidly transitioned into weak westerly winds over the west coast of the middle Korean Peninsula, and the winds to the north of this transition zone were also weak. At that time, a westerly wind flow predominated above 850 hPa over the middle peninsula (not shown).

The mesoscale ridge over the northern Korean Peninsula extending from Wonsan was noticeable in the SLP and 925-hPa height charts throughout the period under consideration (Figs. 2a, 2b, and 3). This stationary ridge will be referred to as the northern ridge hereafter. The southwesterly flow at 925 hPa approaching the KMC (the dotted line for 1000 m over the northeastern Korean Peninsula in Fig. 3a) tended to turn northwestward or northward, whereas the southwesterly flow at 700 hPa tended to cross over the KMC (not shown). As shown in Fig. 3a, relatively cold (marked by "C") and warm (marked by "W") airs were found upstream (around Wonsan) and downstream of the KMC, respectively. These patterns of air temperature were found at all hours presented in Fig. 3 (the

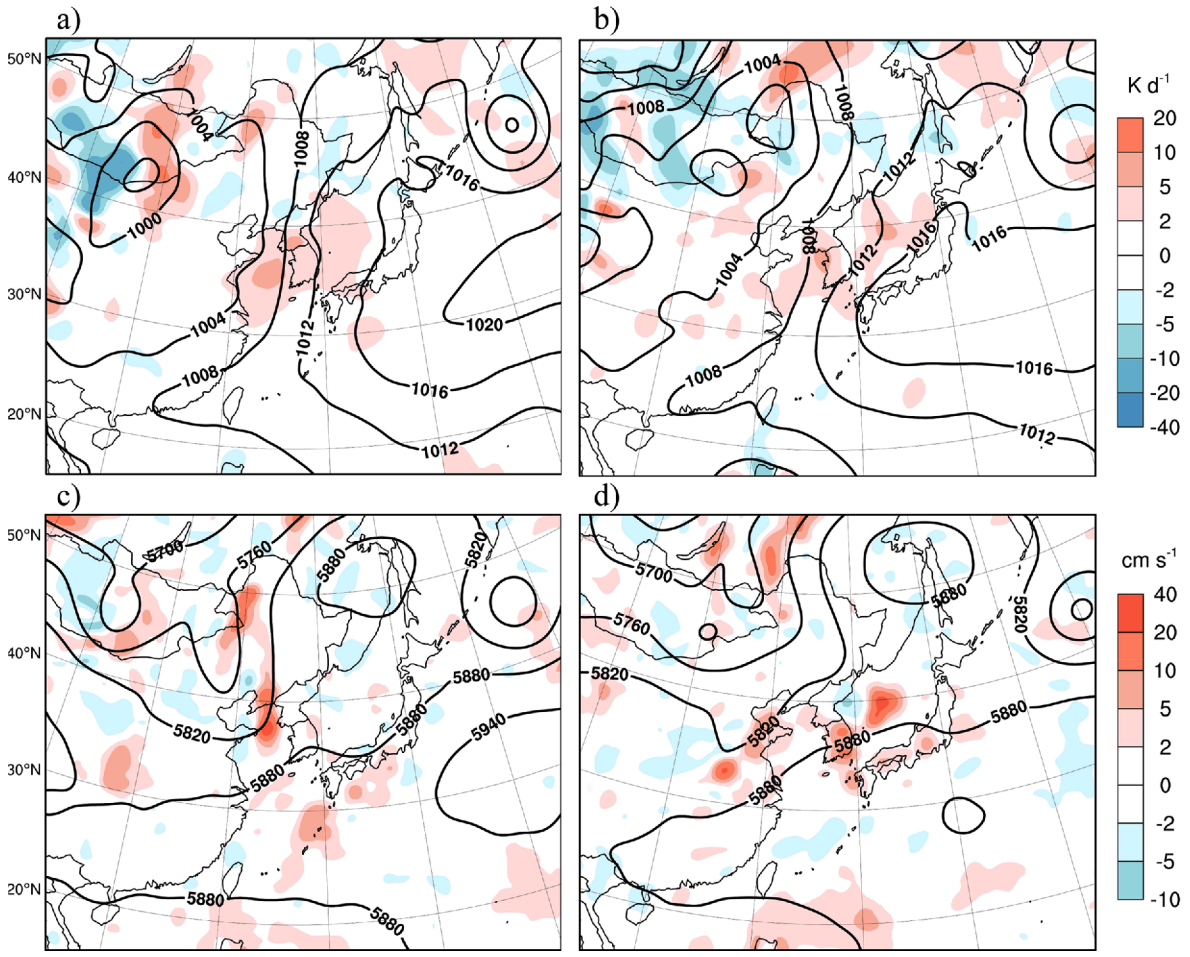

Fig. 2. Sea-level pressure (upper panels, hPa) and 500 hPa charts (bottom panels, gpm) for (a, c) 0000 UTC 26 and (b, d) 0000 UTC 27 July 2011. Temperature advection averaged over the layer of 1000-500 hPa ($-V_g \cdot \nabla T$, K d^{-1}, shaded) and vertical velocity (cm s^{-1}, shaded) at 500 hPa are also shown in the upper and bottom panels, respectively. Fields are from the RDAPS initialized data.

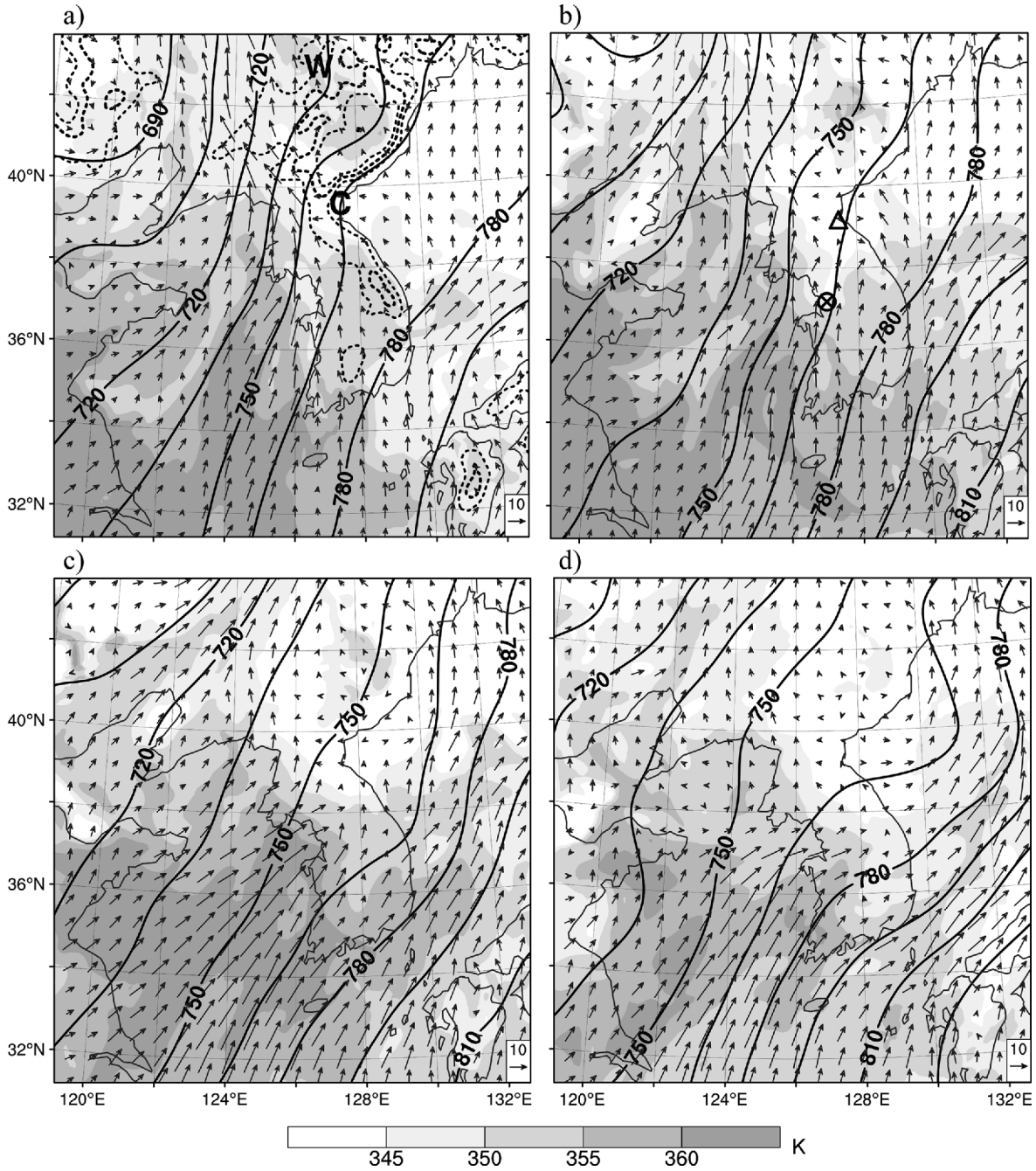

Fig. 3. Geopotential height (gpm, solid lines), θ_e (K, shaded), and wind vectors (m s^{-1}) at 925 hPa for (a) 0600 UTC, (b) 1200 UTC, (c) 1800 UTC 26 July, and (d) 0000 UTC 27 July 2011. The dotted lines in (a) are the contours of the smoothed terrain height for 400, 700, and 1000 m. In (a), the locations of relatively warm and cold air are indicated by "W" and "C", respectively. In (b), the locations of Wonsan and Osan are indicated by "Δ" and "⊗", respectively.

marks "C" and "W" were inserted only in Fig. 3a for simplicity). These air flows and temperature features around the KMC were found mostly below 850 hPa and may indicate the effects of the KMC. Note that a weak height gradient was found over the middle Korean Peninsula at 1800 UTC 26 and 0000 UTC 27 July (Figs. 3c and 3d, respectively). The development of these features (i.e., the northern ridge and the weak height gradient over the middle peninsula) will be examined in relation to terrain effects using a numerical model.

Vertical profiles of observed temperature, dew-point temperature, and wind at Osan station (marked by "⊗" in Fig. 3b) are shown in Fig. 4. Figure 4a shows that the low-level environment was not saturated at 0600 UTC 26 July, and the temperature profile was nearly dry adiabatic below 870 hPa and conditionally unstable in the layer of 720-400 hPa. At 1800 UTC, the air below 850 hPa became more humid due to

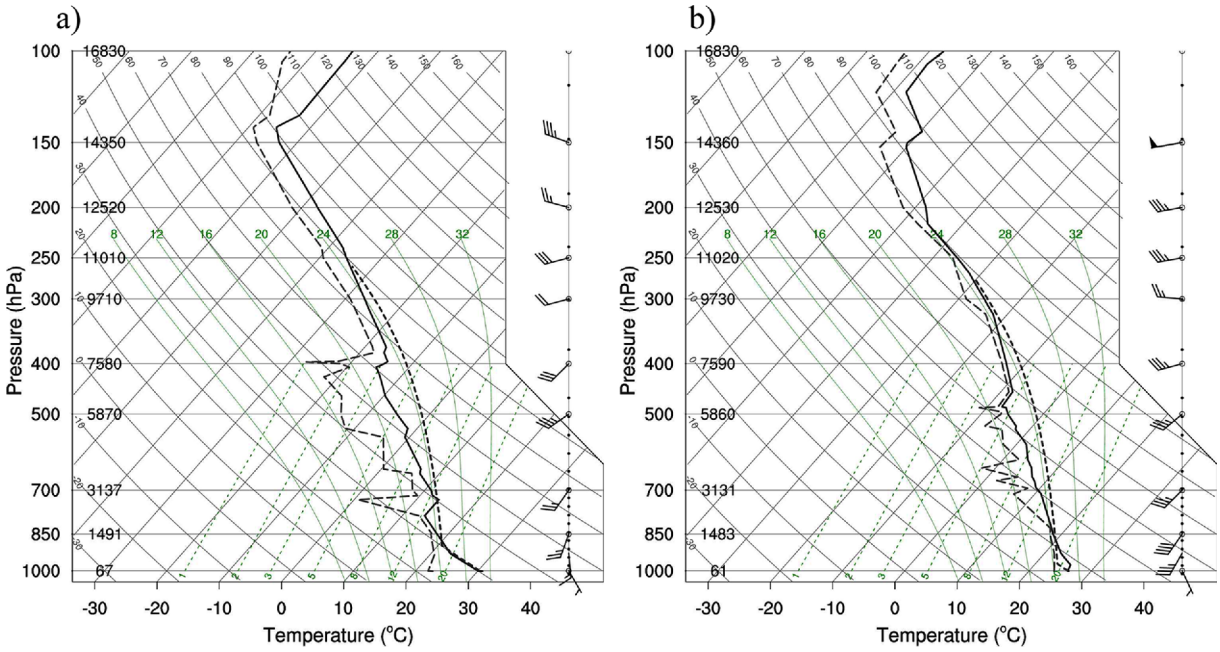

Fig. 4. Profiles of observed temperature (solid line), dew-point temperature (long dashed line), and winds at Osan station for (a) 0600 UTC and (b) 1800 UTC 26 July 2011. Adiabatic lifting of surface air parcel is represented by the short dashed line.

increased dew-point temperature and decreased temperature (Fig. 4b). The increase of dew-point temperature might be due to the transport of moisture by the low-level southwesterly flow from the YS. Convective available potential energy (CAPE) values for surface air parcel increased with time from 372 J kg^{-1} at 1200 UTC 26 to 1722 J kg^{-1} at 0000 UTC 27 July (Table 1). This increase of CAPE was mainly due to the increase of both moisture and temperature near the surface (not shown). The level of free convection (LFC) was low enough for surface air parcel to reach the level by the vertical motion associated with low-level convergence. According to Fig. 4 and Table 1, the thermodynamic condition was sufficiently unstable and that a deep convection could be triggered when air parcels at the surface were raised.

b. Precipitation systems and surface meteorological fields

Satellite (COMS-IR1) images are shown in Fig. 5 from 0600 UTC 26 July to 0000 UTC 27 July at 6-h interval. Strong convective systems developed over the west-middle Korean Peninsula at 0600 UTC 26 July. Cloud-top temperatures lower than −56°C appeared along the southern coast of Hwanghae-do (HHD). And wide area of low cloud-top temperature (lower than −40°C) was extended to the north of the deep convection area. At 1200 UTC, scattered convective clouds were found over the Korean Peninsula with a deep convective system near the coast of HHD. The precipitation system became oriented in the SW-NE direction with convective systems over the western part of the middle Korean Peninsula at 1800 UTC (Fig. 5c), and then the band-type convective systems extended from the west coast in the W-E direction at 0000 UTC 27 July (Fig. 5d).

Table 1. Convective available potential energy (CAPE, J kg^{-1}), Lifted Index (LI), and Level of Free Convection (LFC, m) at Osan (37.10°N, 127.03°E) for 26-27 July 2011.

Time	CAPE	LI	LFC
0600 UTC 26 July	973	−3.2	1089
1200 UTC 26 July	372	−3.5	1582
1800 UTC 26 July	663	−4.5	1210
0000 UTC 27 July	1772	−3.4	453

Figure 6 shows the observed SLP from synoptic weather stations, surface winds from both synoptic stations and AWSs, and composite radar reflectivity at 1.5 km. Isobars were not drawn in areas for which data were not available (e.g., the east and west coasts). At 0000 UTC 26 July, several convective systems from the YS approached the west coast of the north-to-middle Korean Peninsula (Fig. 6a). At 0300 UTC, a cluster of strong convective systems moved to the southern coast of HHD (Fig. 6b) and a mesoscale ridge and trough pair developed over the middle Korean Peninsula. Surface winds over the coast of southern HHD and Gyeonggi Bay were mainly from the south or southeast.

At 0600 UTC, strong convective systems developed mainly along the southern coast of HHD and on the west coast to the northwest of Seoul (Fig. 6c), and a broad area of stratiform rainfall was present to the northeast. The mesoscale ridge over HHD showed a strong development in a SW-NE direction, and the mesoscale trough to its south also became well defined. The ridge over HHD will be referred to as the middle ridge hereafter. Surface easterly winds occurred along the southern

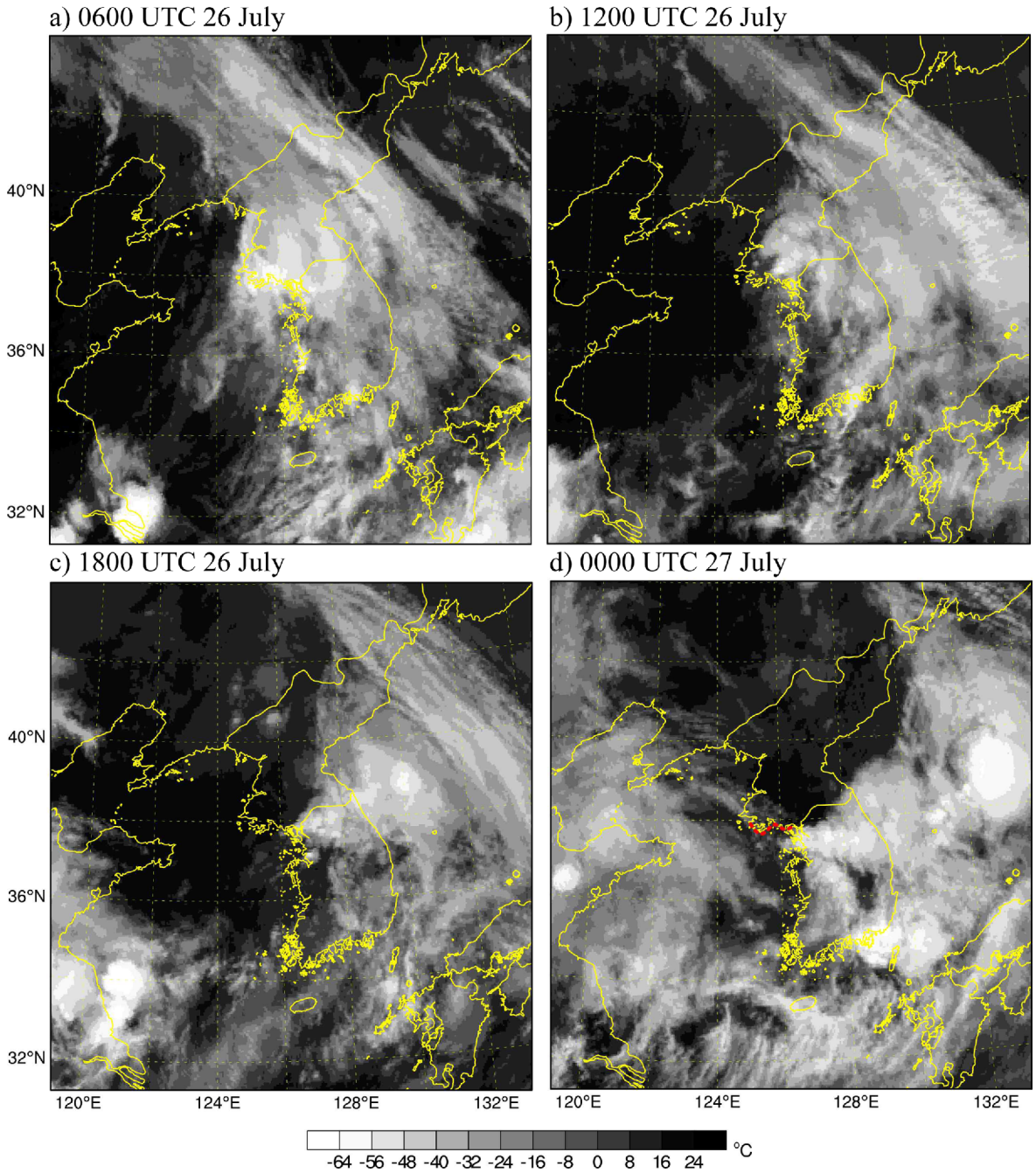

Fig. 5. COMS infrared (IR1) images for (a) 0600, (b) 1200, and (c) 1800 UTC 26 July 2011, and (d) 0000 UTC 27 July 2011. Southern coast of HHD is indicated by a red dashed line in (d).

side of the ridge (i.e., along the southern coast of HHD and northern GGD), whereas surface southerly winds prevailed over the sea to the south of the ridge. As a result of this wind distribution, low-level flows may have converged along the southern side of the middle ridge, which was also indicated by the strong convective systems over this area in Fig. 6c. The surface winds along the southern side of the ridge were likely affected by convective systems (i.e., surface outflows). At this time, airflows at levels above 850 hPa ranged from southerly at 850 hPa to southwesterly at 500 hPa. These upper-level winds appeared to have transported clouds toward the north and northeast, which resulted in a wide area of stratiform rainfall in the northern Korean Peninsula. The middle ridge shifted its location after 0600 UTC. However, the middle ridge and trough pair persisted throughout the period shown in Fig. 6. At 1800 UTC, the middle ridge was enhanced near the Wonsan area, and weak surface northeasterly winds were found over the inland area to the northeast of the major convective

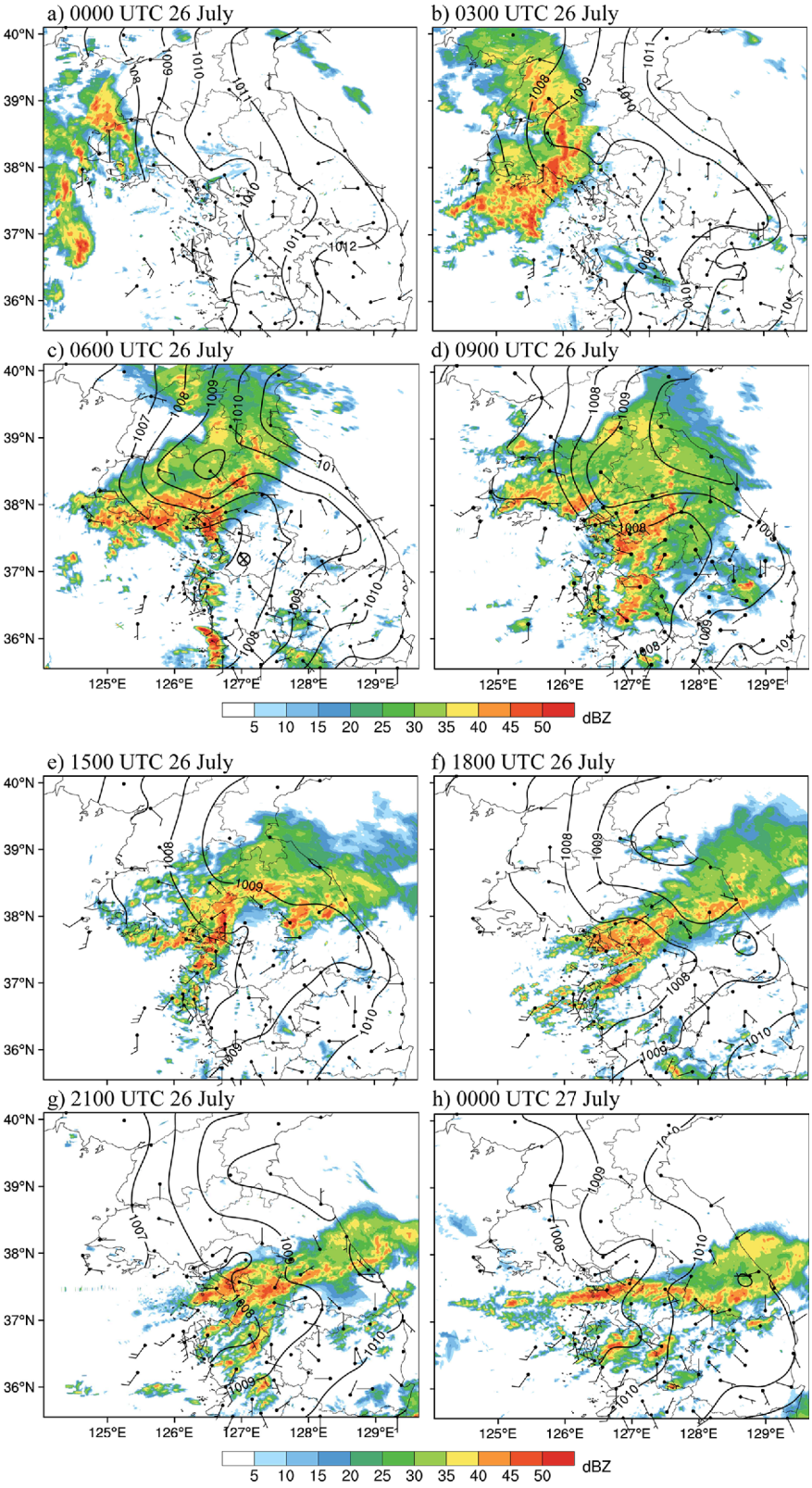

Fig. 6. Sea-level pressure (hPa, solid lines), surface winds (m s^{-1}), and composite radar reflectivity at 1.5 km (dBZ, shaded) over the middle Korean Peninsula for (a) 0000 UTC, (b) 0300 UTC, (c) 0600 UTC, (d) 0900 UTC, (e) 1500 UTC, (f) 1800 UTC, (g) 2100 UTC 26 July, and (h) 0000 UTC 27 July 2011. The symbol "⊗" in (c) indicates the location of Osan station.

systems near the west coast and Seoul (Fig. 6f). At the same time, relatively strong surface southwesterly winds were present over the west coastal area. A similar wind pattern also occurred at 2100 UTC (Fig. 6g).

The echo pattern changed with time. It began as a pattern of strong convective systems along the coasts of southern HHD and GGD with broad stratiform clouds to the north on 0600-1200 UTC 26 July (stage 1) (Figs. 6c and 6d). This pattern then changed to a medium band of precipitation extending from the west to the east coast of the middle Korean Peninsula in a SW-NE direction during 1500-2200 UTC (stage 2) (Figs. 6f and 6g). During stage 2, the majority of the strong convective systems occurred over the west-middle Korean Peninsula. An examination of the radar images indicated that small cells developed over Gyeonggi Bay and moved northeastward to form bands of convection. The convective bands tended to aggregate over the west-middle Korean Peninsula. After 2100 UTC, a narrow W-E convective band developed over Gyeonggi Bay. Convective systems within the band intensified as they moved toward Seoul (Fig. 6h). The systems produced intense heavy rainfall over the Seoul metropolitan area from 2200 UTC 26 to 0100 UTC 27 July 2011 (stage 3) (Fig. 6h). Surface winds along the band over the coast indicate the presence of a narrow convergence zone along the band. The HPSs during this period were studied by Lee et al. (2014a).

The accumulated rainfall amount during the 18-h period of 0600 UTC 26-0000 UTC 27 July 2011 was close to the 24-h rainfall amount shown in Fig. 1 except for in HHD, where the rainfall started after 0100 UTC 26 July.

c. Factors for the development of heavy precipitation systems

As mentioned above, the pattern of precipitation systems distinctly evolved during the 3 stages. In this study, we focused on the first two stages to explain (1) the formation of the middle ridge over HHD and the role of the ridge in the development of the HPSs in stage 1 (i.e., 0600-1200 UTC 26 July) and (2) the environment and development of the medium-sized band of precipitation in stage 2 (1500-2200 UTC).

(1) Stage 1

We will first address the development of the middle ridge using surface observations. Figure 7a shows the three-hour changes in the SLP and surface-air temperature during 0300-0600 UTC (1200-1500 LST) 26 July. Sea-level pressure decreased over the Korean Peninsula except at the Singye station (38.50°N, 126.53°E) (marked by "□" in Fig. 7a). The SLP decrease could be attributed to the diurnal variation in the SLP on the continental and local scale. For example, surface-air temperature at Cheongju station (marked by "○" in Fig. 7a), where the precipitation systems did not pass over, increased until 0600 UTC and then decreased thereafter (Fig. 7b). Trend of SLP at the station was opposite to that of the temperature with a time lag of 3 hours. Similar diurnal variations of surface-air temperature and SLP were found at other stations where

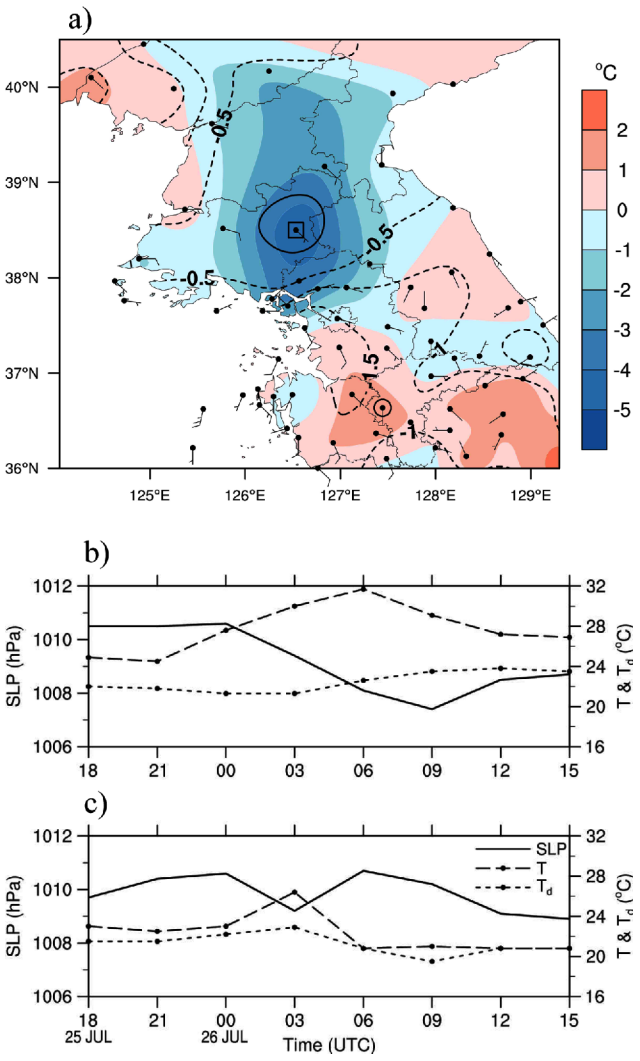

Fig. 7. (a) Three-hour changes of SLP (hPa, solid and dashed lines for positive and negative values, respectively) and surface air temperature (°C, shaded) for 0300-0600 UTC 26 July 2011. (b,c) Time-series of SLP (hPa, solid line), surface-air temperature (°C, dashed line), and dew-point temperature (°C, dotted line) at (b) Cheongju (36.64°N, 127.44°E) and (c) Singye (38.50°N, 126.53°E) station. The locations of Cheongju and Singye stations are indicated by "○" and "□" in (a), respectively. Surface winds (m s^{-1}) in (a) are for 0600 UTC 26 July 2011.

increase of surface air temperature was found during 0300-0600 UTC (not shown). However, at Singye station, a significant SLP increase occurred during 0300-0600 UTC when surface-air temperature decreased by about 4°C (Fig. 7c). Because the period includes the time at which the maximum surface air temperature may occur, the large temperature decrease over HHD could have been caused by factors other than surface forcing. A possible cause of the cooling could have been the evaporation of rain water. As shown in Fig. 7c, the air near the surface was not saturated at 0300 UTC and a broad stratiform precipitation was present around the Singye station during 0300-0600 UTC (see Figs. 6b and 6c). Because

rain water evaporation can occur through a deep layer below clouds, Fig. 7c may not provide a clear proof of evaporative cooling. But, it confirmed that surface air was not saturated and rain water evaporation could have occurred at the Singye station. The effects of evaporative cooling will be discussed later using a numerical simulation. The area in which the SLP increased over HHD coincided with the middle ridge, whereas the area in which the SLP decreased over much of the middle Korean Peninsula coincided with the trough. Thus, the meso-scale ridge and trough pair over the middle Korean Peninsula developed as the middle ridge responded to the cooling of the low-level air in the daytime when the SLP decreased over the Korean Peninsula.

Kim and Lee (2006) also found that a cold pool and warm sectors were collocated with the meso-high and meso-low pressure systems, respectively, in a case study of heavy rain occurred over the middle Korean Peninsula on 25-27 July 1996. The authors suggested that the cold pool could persist for many hours after the decay of a MCS and played a role in triggering a storm in the initiation phase of successive convective storms. However, they did not explain the cold pool in detail such as the processes of its development and triggering of convective systems.

According to this study, the middle ridge over HHD was accompanied by an easterly flow along its southern side; consequently, a convergence zone was induced between the low-level easterly flow and the southerly flow from the YS. Since the low-level easterly might be due to the outflow associated with a cold pool over HHD which developed in response to the cooling by evaporation of rain water, it might be said that the strong convective systems along the southern coast of HHD was triggered by cold-air outflow. This will be discussed further in section 3b. The cloud systems at a higher levels appeared to be transported toward the NNE and NE by the upper-level winds.

(2) Stage 2

In stage 2, a medium band of precipitation extended from the west to east coasts in a SW-NE direction over the middle Korean Peninsula and major convective systems developed over the western part of the middle Korean Peninsula. In this section, we examine the factors associated with the development of the HPSs over the western part of the middle Korean Peninsula and the cause of the transition of precipitation-system patterns from the stage-1 type to the medium-band type.

During this stage, the mesoscale ridge-trough pattern still occurred over the middle Korean Peninsula, and surface convergence could be found over GGD in a northeasterly winds over the inland region and southwesterly winds over the west coast (Fig. 6f), and the southwesterly airflow from the YS at 925 hPa also rapidly weakened over the west coastal area of GGD (Fig. 3c). Figure 8 shows the flow and divergence structures associated with the precipitation band at 1800 UTC from the RDAPS initialized data. Significant convergence was found at 850 hPa along the precipitation band over the middle

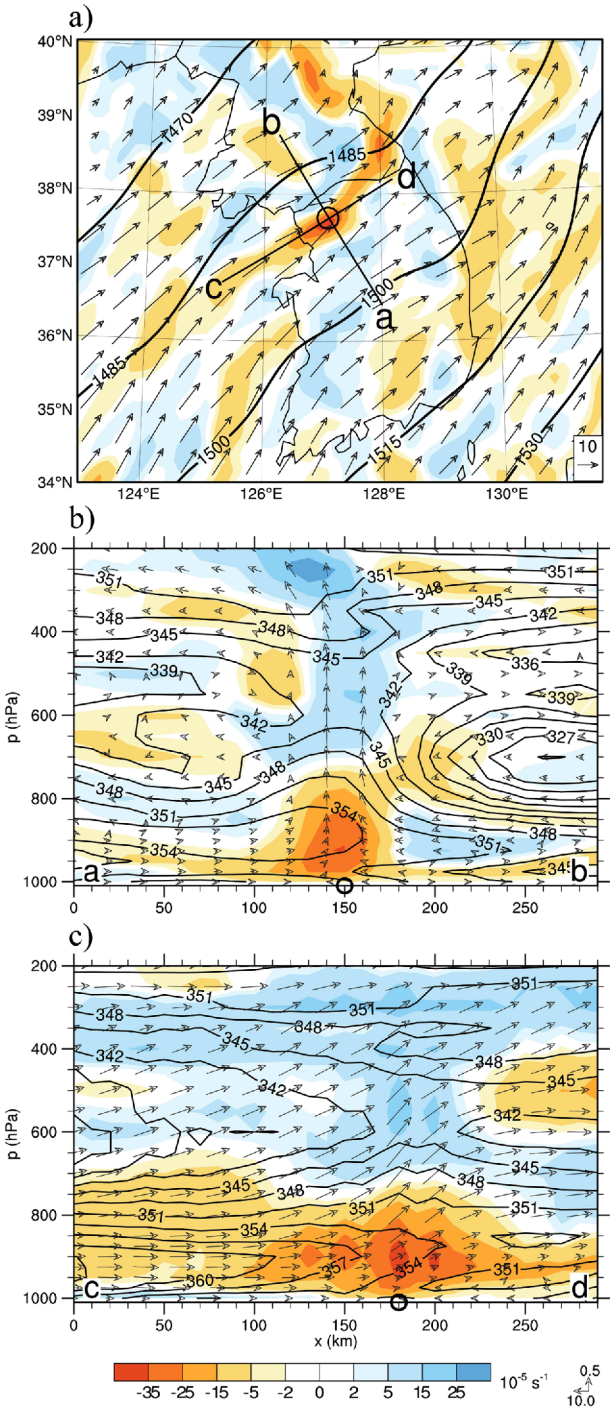

Fig. 8. (a) Horizontal divergence (10^{-5} s^{-1}, shaded) and geopotential height (m, solid lines) at 850 hPa, and cross sections of the horizontal divergence (10^{-5} s^{-1}, shaded), θ_e (K, solid lines), and in-plane winds (m s^{-1}, vector) along the line (b) a-b and (c) c-d for 1800 UTC 26 July 2011. The fields are from RDAPS initialized data. Circles in (a) and on the abscissa of (b) and (c) indicate the intersection point of the cross section planes.

Korean Peninsula (Fig. 8a). This band of strong convergence appeared to contain the effect of strong convection. Two different cross-sections of the airflow and horizontal divergence

are shown: one across the band (Fig. 8b) and the other along the band (Fig. 8c). The cross-section across the band shows a relatively strong convergence that exceeded -15×10^{-5} s^{-1} below approximately 800 hPa, and a strong upward motion appeared from the convergent layer to the upper troposphere (Fig. 8b). The cross-section along the band also indicated a deep layer of convergence (Fig. 8c). The depth of the convergent layer decreased from a deep layer below 700 hPa over the sea to a shallow layer below 850 hPa over the middle Korean Peninsula. Strong convergence appears in the 850-950 hPa layer over the inland region near the coast. The horizontal convergence along the c-d line in Fig. 8c consists of in-plane and cross-plane wind components. Calculation indicated that the cross-plane wind component dictated the convergence above 925 hPa at the intersection point, while both components were similarly important for convergence below 925 hPa (not shown). Importance of cross-plane wind component above 925 hPa could be due to the effects of convective band which was parallel to the cross section. In the meantime, the significant convergence of in-plane winds below 925 hPa in the presence of convective band may indicate that the rapid decrease of wind speed toward the inland area at low levels is an important cause of the low-level convergence.

As shown in Fig. 8b, the horizontal winds toward the convergence band were weak on both sides of the strong upward motion. Therefore, the winds were nearly parallel to the precipitation band throughout the troposphere, which might help explain the transition of the precipitation pattern from stage 1 to stage 2. The transition can be explained by the horizontal extension of strong convective systems and upper-level (i.e. 850-500 hPa) wind direction. In stage 1, development of strong convective systems tended to occur along the coast of southern HHD and GGD (Figs. 6c and 6d), and upper clouds were moved toward the NNE~NE by the upper-level winds, which crossed the coastline. In stage 2, major convective systems were spread over a relatively small area of the west-middle Korean Peninsula and northeastward movement of precipitation system along the upper-level southwesterly winds resulted in a medium band of precipitation system across the middle Korean Peninsula (Figs. 6f and 6g). The orientation change of the precipitation band from SW-NE direction at 1800 UTC 26 July to about W-E direction at 0000 UTC 27 July (Fig. 6h) was also consistent with the change of upper-level wind direction (not shown).

3. Numerical investigation of the development of the mesoscale ridges and heavy precipitation systems

The observational analysis indicated that two mesoscale ridges developed during the heavy rainfall period under consideration: one ridge in the middle Korean Peninsula (i.e., the middle ridge) and the other ridge in the northern Korean Peninsula (i.e., the northern ridge). The middle ridge over HHD developed during the daytime on 26 July because of the cooling of the low-level air, and the development of northern ridge was related to the effects of the KMC.

In this section, we discuss the formation processes for these mesoscale ridges using the Weather Research and Forecasting Model Version 3.5.1 (WRF V3.5.1) (Skamarock et al., 2008). Five numerical experiments were performed (Table 2). The effects of evaporative cooling, the land-sea contrast of the surface friction, and the diurnal heating of the land surface on the formation of the middle ridge and convection over southern HHD were investigated in three sensitivity experiments: noEC, HoSF, and wkSUN, respectively. The FTKP experiment, in which the entire Korean Peninsula was assumed to have a flat terrain, was employed to investigate the terrain effects of the mountains on the formation of the northern ridge and the environment of HPS development over the middle Korean Peninsula. The land-use type adopted for the FTKP simulation was identical to that of the CTRL simulation. All numerical simulations were conducted for a 30-h period starting from 0000 UTC 26 July 2011 in the same model domains using the same physics scheme combinations. The model domains and the topography are shown in Fig. 9.

A one-way nested grid system was used for three domains with 22.5-, 7.5-, and 2.5-km grids, for which time steps of 60, 20, and 10 s are used, respectively. The three domains contained 150×150, 301×331, and 400×430 horizontal grid points, respectively, and all domains had 41 vertical layers up to 50 hPa with a terrain-following eta (η) coordinate. Additional experiments were also conducted to ascertain the appropriateness of the present model configuration for the control simulation (i.e., two experiments to check the sensitivity of the simulation to the nesting method and model-top height): one using a two-way nested grid system and the other placing the model top at 10 hPa. It was found that the results from the two experiments were very similar to those from the control simulation for the present case. The physics schemes included

Table 2. Summary of the numerical experiments.

Name	Description
CTRL	Control simulation
noEC	No evaporative cooling: latent cooling due to the evaporation of rainwater is switched off.
HoSF	Homogeneous surface friction: roughness length for momentum of land surface is assumed to be the same as the ocean surface roughness (i.e., 0.01 cm).
wkSUN	Solar constant is reduced to 10 W m^{-2}. (Solar constant for CTRL is 1370 W m^{-2}.)
FTKP	The terrain height over the Korean peninsula is set to 1 m.

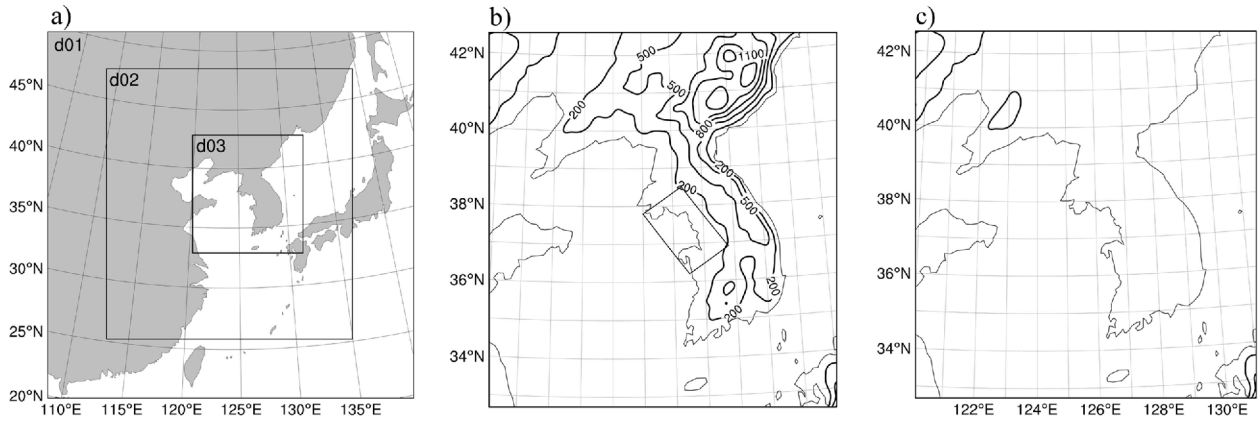

Fig. 9. (a) Domain of the numerical experiments, and the topography within domain 3 (d03) for (b) the control (CTRL) and (c) the flat Korean Peninsula (FTKP) experiments. The contour starts from 200 m and has an interval of 300 m. The box in (b) indicates the region in which the upstream flow parameters were calculated.

the Kain-Fritsch cumulus scheme (Kain, 2004), the WRF single-moment 6-class (WSM6) scheme (Hong and Lim, 2006), the updated rapid radiative transfer model (RRTMG) longwave and shortwave radiation schemes (Iacono et al., 2008), and the Mellor-Yamada-Janjić (MYJ) planetary boundary layer scheme (Janjić, 1994). Cumulus parameterization was used only in the two domains with coarser grids. Six-hourly NCEP climate forecast system reanalysis (CFSR) data ($0.5^{o} \times 0.5^{o}$) (Saha et al., 2010) were used for the initial and boundary conditions.

a. Simulation of the middle ridge and heavy precipitation systems

Figure 10 shows the simulated SLP, the surface winds (at 10 m) and the reflectivity at 1.5 km. The middle ridge began developing on the west coast, where the convective systems from the YS first arrived (Fig. 10a). The development continued inland as the precipitation systems extended toward the east. The simulation reproduced the middle ridge and trough pair over the middle Korean Peninsula at 0600 UTC (Fig. 10b). The simulated ridge developed over HHD, and a weak surface easterly flow appeared along its southern side, as also seen in the observational analysis (Fig. 6c). The ridge was maintained until 1200 UTC and then the ridge-trough pattern became less clear, which is inconsistent with the observational analysis (Figs. 10e and 10f). After 1200 UTC, a SW-NE-oriented band of MCSs developed over the middle Korean Peninsula and moved southward at a faster rate than was indicated by the observational analysis, and its location at 1800 UTC was approximately 50 km south of the observed band (Fig. 10f). However, the simulated surface wind at 1800 UTC showed an important observed feature: a rapid transition from a relatively strong southwesterly wind to a near calm on the west coast (Fig. 10f). However, the simulation did not show the observed northeasterly surface winds over the inland area (see Fig. 6f).

The simulated reflectivity pattern was consistent with the observations in the following features: (1) the development of convective systems elongated in the N-S direction along the west coast of the northern Korean Peninsula at 0300 UTC (Fig. 10a), (2) the development of strong convective systems along the southern side of the middle ridge at 0600 UTC (Fig. 10b), and (3) the continued presence of HPSs over the middle Korean Peninsula (Figs. 10c and 10d). However, the simulated band of MCSs moved southward after 1200 UTC, which was inconsistent with the trend indicated by the observational analysis. And the simulated reflectivity for the convective systems was generally stronger than the observations. The stronger simulated reflectivity may be mainly due to the reason that the simulated convective systems were stronger than the observation. This may be supported by the results shown in Fig. 11b, in which simulated area-average rainfall amount was larger than the observed amount during 0300-1600 UTC.

Figure 11a shows the simulated 18-h rainfall amounts from the CTRL experiment. Simulated rainfall amount was greater than 100 mm over a wide area of the middle Korean Peninsula, with the heavier rainfall exceeding 300 mm to the north and east of Seoul. This simulation is similar to the observations in Fig. 1. However, the simulated rainfall amount over east-central GGD, central Gangwon-do and the east coast was less than the observed value. The large simulated amount of rainfall south of 37°N was mainly caused by the southward shift of simulated HPSs after 1800 UTC 26 July. This discrepancy from the observed behavior after 1800 UTC may have been caused by the accumulation of errors in the simulated pressure field and precipitation systems, which are sensitive to each other.

Time-series of area-averaged hourly rainfall amounts from the observations and the CTRL simulation are shown in Fig. 11b. Both observed and simulated hourly rainfall amounts were interpolated to 201×201 grid points within the domain of 36.0-38.5°N and 125.5-129.0°E where sufficient number of observation stations were available. And then the area-

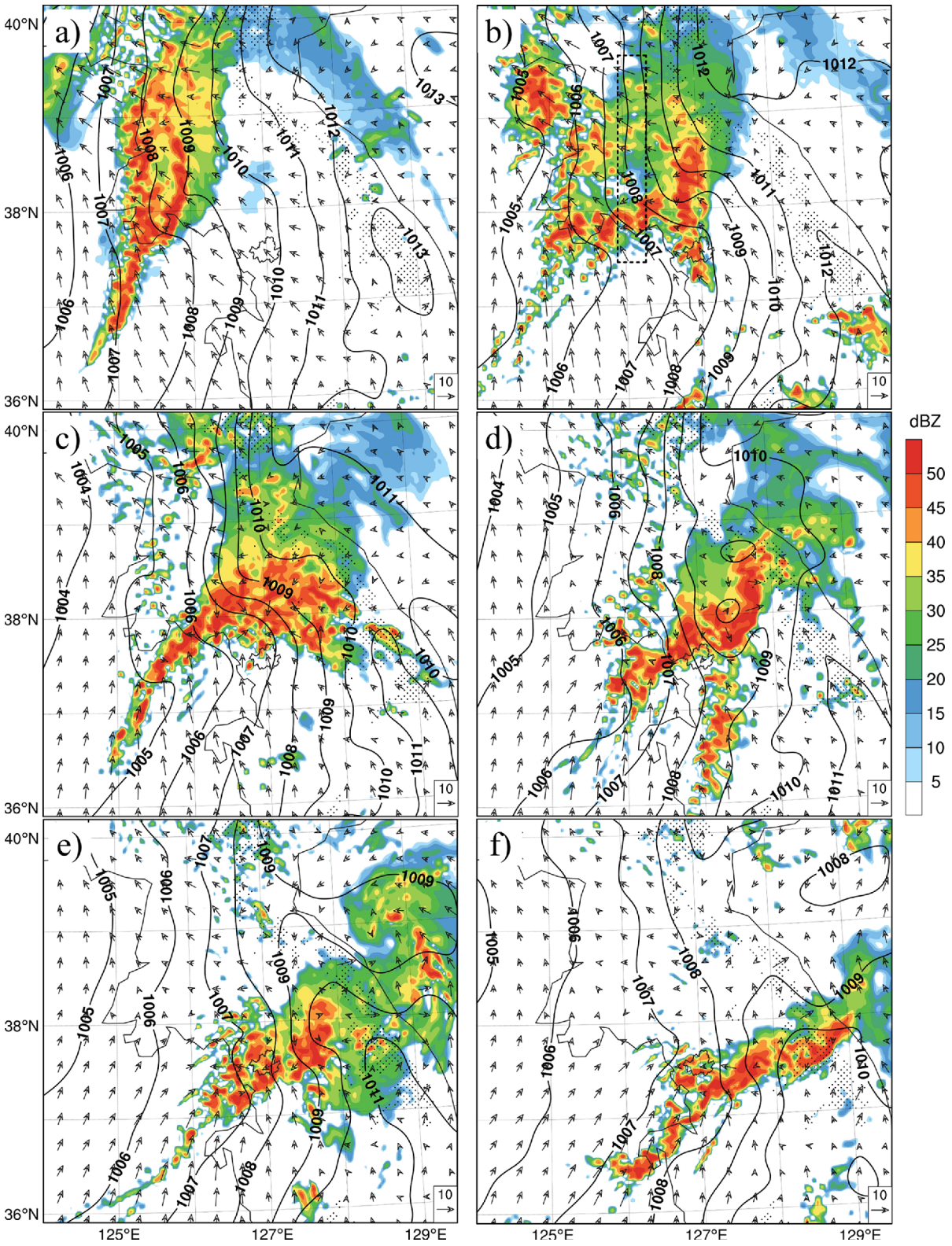

Fig. 10. Simulated SLP (hPa, solid lines), surface winds at 10 m (m s^{-1}, vectors), and reflectivity at 1.5 km (dBZ, shaded) for (a) 0300 UTC, (b) 0600 UTC, (c) 0900 UTC, (d) 1200 UTC, (e) 1500 UTC, and (f) 1800 UTC 26 July 2011. Results with a 2.5-km grid size. The dotted box in (b) represents the area where averaged cross section in Fig. 12 was obtained.

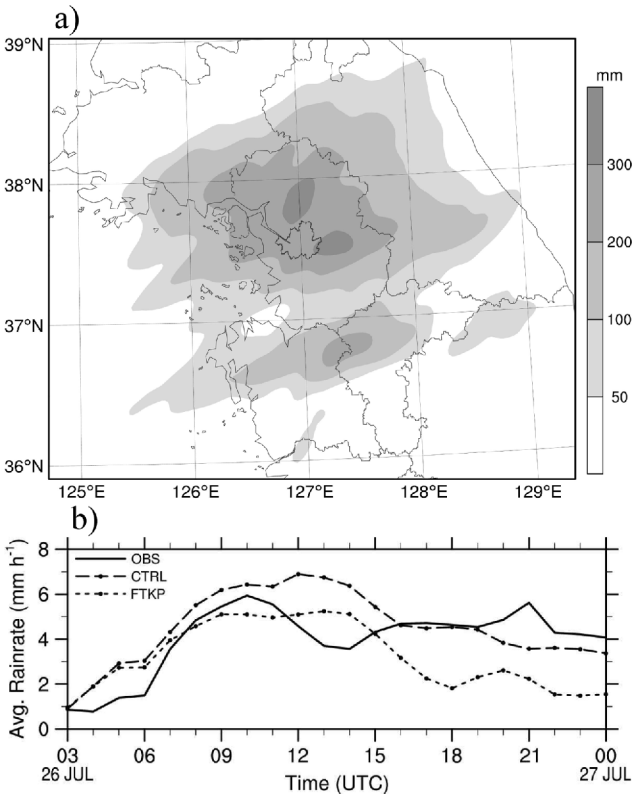

Fig. 11. (a) Accumulated rainfall amount (mm) from the CTRL experiment for 0600 UTC 26-0000 UTC 27 July 2011 and (b) time-series of area-averaged hourly rainfall amount (mm h^{-1}) from the observations (solid line), CTRL (dashed line) and FTKP experiments (dotted line).

averaged hourly rainfall amount was obtained by averaging the grid values over the domain. The trend of simulated hourly rainfall amount was similar to that of observed rainfall amount until 1100 UTC. However, simulated rainfall amount was significantly larger than the observation during 1200-1500 UTC, and the secondary peak at 2100 UTC was not simulated.

The observational analysis suggested that the middle ridge over HHD and its associated easterly flow provided a lifting mechanism for the low-level southerly airflow from the sea (Fig. 6). This hypothesis was investigated using the simulated results. Figure 12 shows a cross-section of the horizontal divergence, in-plane winds, sum of cloud water and cloud ice mixing ratios, and rain water mixing ratio. The values were averaged over the rectangular box in Fig. 10b in the W-E direction. A strong horizontal convergence that exceeded -40×10^{-5} s^{-1} was found at levels below 2 km over the coast (the coastline is marked by a square on the abscissa), and a strong ascent and deep convective clouds were found over the area (Fig. 12). The low-level convergence and associated rising motion were sufficient to lift the low-level air from the south above the LFC, which was at approximately 1500 m (not shown). The figure also indicates the northward advection of the upper-level clouds, under which a moderate amount of rain water was present.

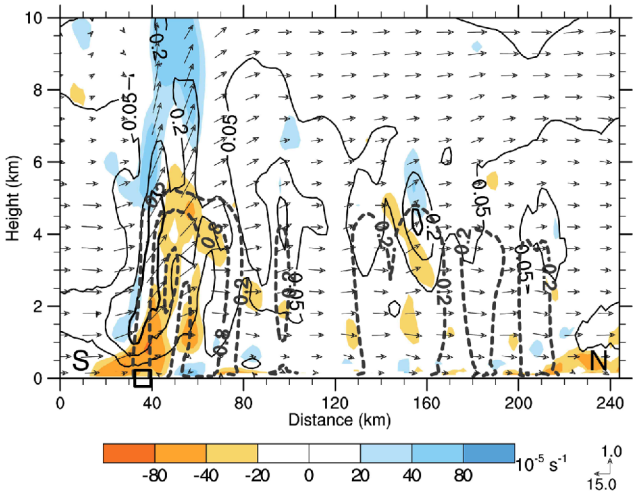

Fig. 12. Cross sections of the simulated horizontal divergence (10^{-5} s^{-1}, shaded), sum of cloud water and cloud ice mixing ratios (g kg^{-1}, solid lines for 0.05, 0.2, and 0.4), rain water mixing ratio (g kg^{-1}, gray dashed lines, for 0.2, 0.8, and 1.6), and in-plane winds (m s^{-1}, vectors) for 0600 UTC 26 July 2011. The values represent the averages across the domain in the W-E direction (domain location is shown in Fig. 10b). The square on the abscissa indicates the location of the coast line.

b. Physical factors for the development of the middle ridge and trough

The simulated fields of the noEC experiment are shown in Fig. 13 to demonstrate the evaporative cooling effects. The middle ridge over HHD did not develop at 0600 UTC (Fig. 13a), and a relatively broad trough appeared over the middle Korean Peninsula, including HHD, at 1200 UTC (Fig. 13b). The pattern of the precipitation systems was also greatly different from that of the CTRL simulation. Convective development along the southern coast of HHD did not appear because of the absence of the middle ridge and the associated easterly flow at low levels (Fig. 13a). Instead, N-S oriented precipitation systems tended to develop over the middle Korean Peninsula and moved eastward. These features indicate that evaporative cooling was a crucial factor for the formation of the middle ridge, which could result in the sustained development of the HPSs over the west-middle Korean Peninsula.

The effect of evaporative cooling was extracted by determining the differences in the temperature, SLP and winds between the CTRL and noEC simulations at 0600 UTC 26 July (Fig. 14a). The temperature difference in this figure represents the average of the differences in the lowest 200-hPa layer. The differences in the temperature and SLP were well correlated, and an increased SLP was found in areas where evaporative cooling occurred. Note the significant outflow over southern HHD and northern GGD, which suggests that the development of surface easterly winds along the southern side of the ridge was mainly caused by the outflow associated with the cold pool over the inland HHD. Figure 14b shows a vertical cross-section of the sum of cloud water and cloud ice

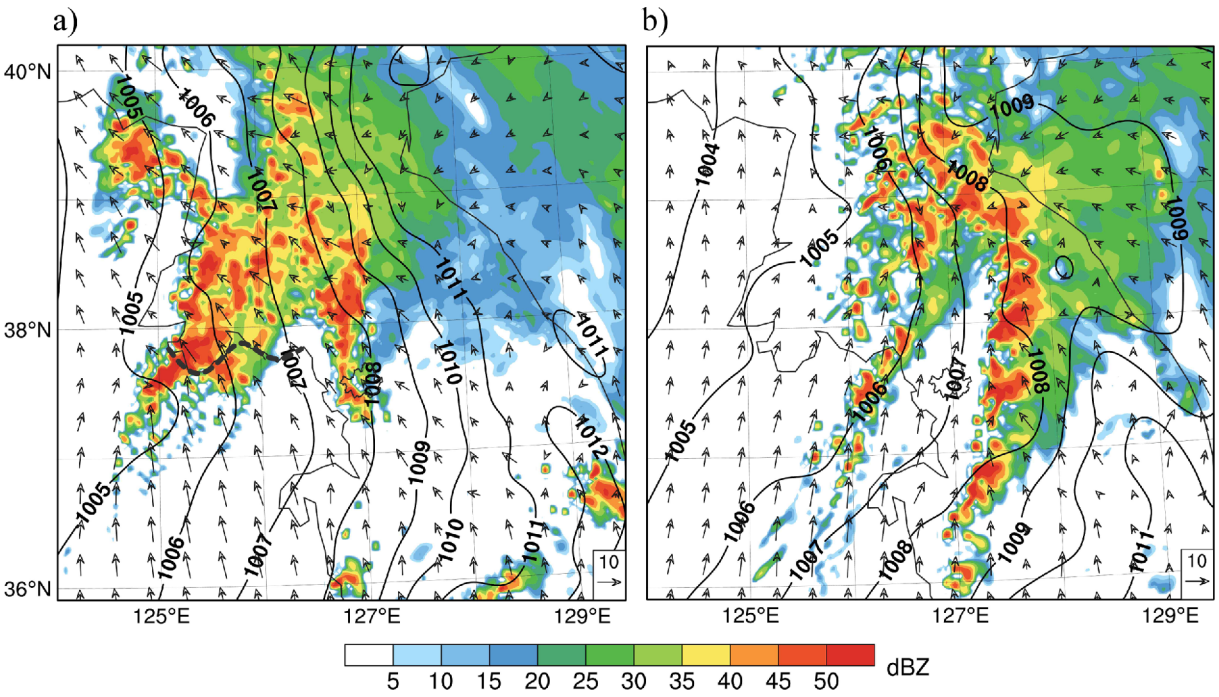

Fig. 13. Same as Fig. 10 except for the noEC simulation: (a) 0600 UTC and (b) 1200 UTC 26 July 2011. Southern coast of HHD is indicated by a gray dashed line in (a).

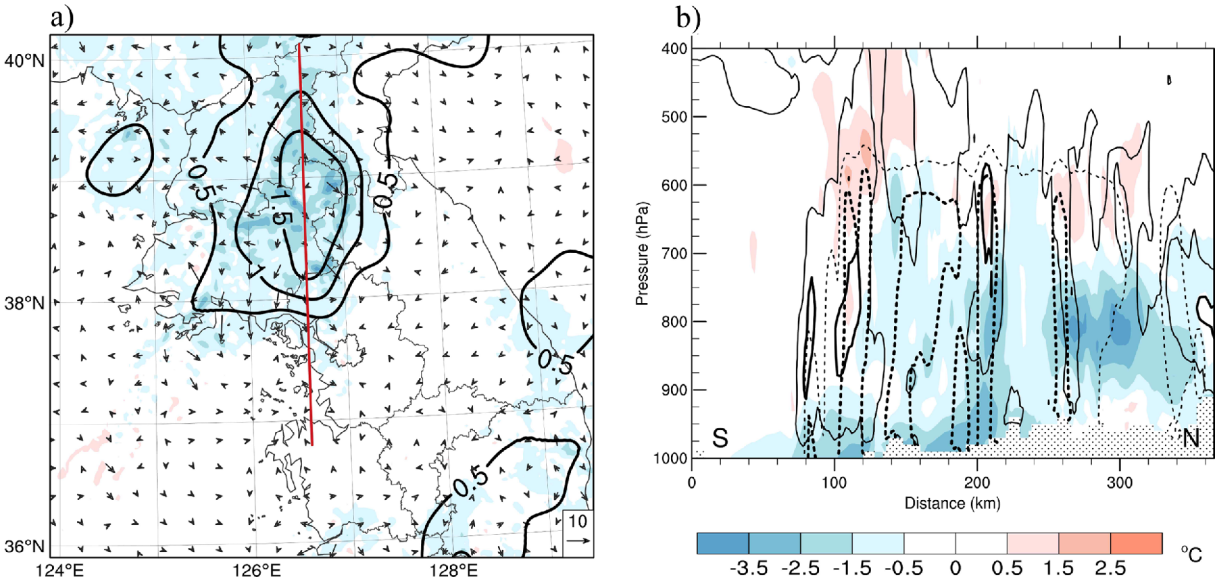

Fig. 14. (a) Difference of simulated SLP (hPa, solid lines) and temperature (°C, shaded) between the CTRL and noEC simulations, and (b) the vertical cross section of the sum of cloud water and cloud ice mixing ratios (thin and thick solid lines for 0.02 and 0.5 g kg^{-1}, respectively) and rain water mixing ratio (thin and thick dashed lines for 0.1 and 0.4 g kg^{-1}, respectively) from the CTRL simulation and the temperature difference (°C, shaded) between the CTRL and noEC simulations for 0600 UTC 26 July 2011. The location of the cross section is shown in (a). The temperature difference in (a) is the average difference in the lowest 200 hPa layer.

mixing ratios and the rain water mixing ratios from the CTRL simulation and the temperature differences between the CTRL and noEC simulations along the line in Fig. 14a. A deep convective cloud was found on the southern side of the precipitation system, and to the north of this deep cloud, the clouds principally occurred in the layer above 600 hPa, and significant amounts of rain water were contained below these clouds. The rain water mixing ratio was greater than 0.3 g kg^{-1}

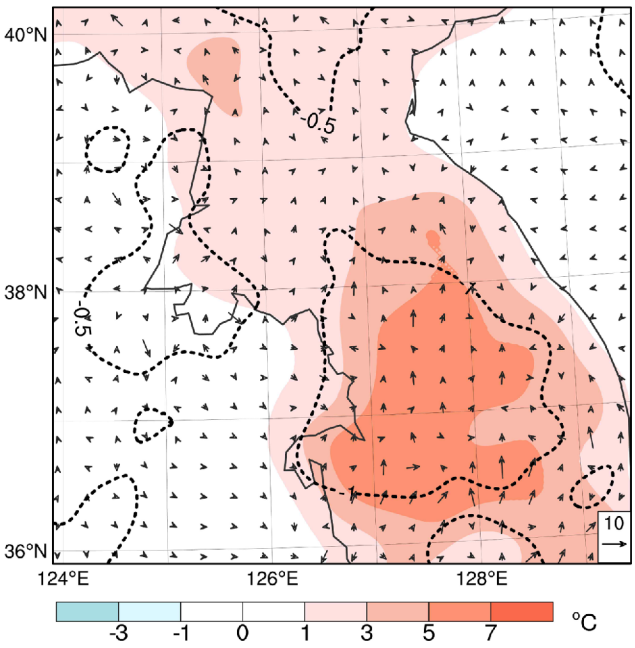

Fig. 15. Difference in the SLP (hPa, solid and dotted lines for positive and negative differences, respectively), 10-m winds (m s^{-1}, vectors), and temperature (K, shaded) between the CTRL and wkSUN simulations for 0600 UTC 26 July 2011.

over much of the rainy area. A negative temperature difference was found over the entire area below the clouds, and relatively large differences were found in the layer between the surface and 700 hPa.

Compared with the noEC simulation, the middle ridge and strong convective systems over the southern coast of HHD at 0600 UTC appeared in all other sensitivity experiments (e.g., Fig. 16a) and the abrupt change in the surface winds still occurred along the southern coast of HHD.

Neglecting the diurnal heating and land-sea contrast of surface friction did not significantly affect the development of the HPSs. However, an important effect of diurnal heating is worth mentioning, and it can be explained using Fig. 15. A large positive temperature difference of 5-7 K was found over the inland area between 36°N and 38°N, where HPSs were not found at 0600 UTC 26 July in the CTRL simulation. A weak decrease in the SLP was found in the area where this large positive temperature difference appeared. Thus, the solar heating of the land surface may have partially contributed to the development of the mesoscale trough over the middle Korean Peninsula as the evaporative cooling primarily affected the SLP distribution.

The sensitivity experiments showed that (1) evaporative cooling was the major factor that contributed to the development of the middle ridge and surface easterly along the southern side of the ridge, (2) the land-sea contrast of surface friction was not important for the development of the HPSs, and (3) the diurnal heating of land surface partially contributed to the development of the trough over the middle Korean Peninsula.

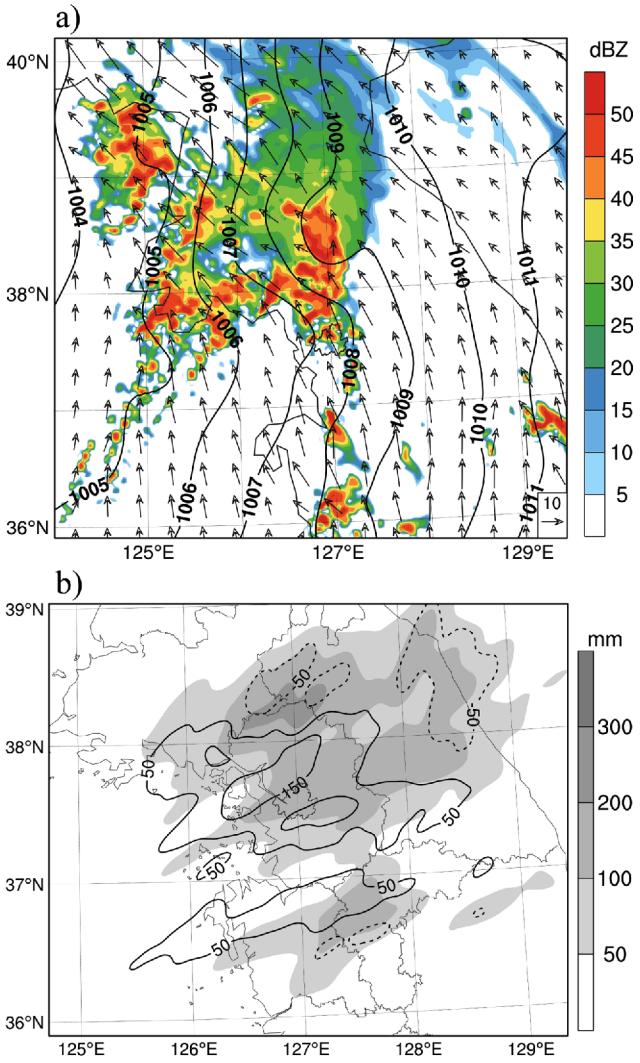

Fig. 16. (a) Simulated SLP (hPa, solid lines), surface winds at 10 m (m s^{-1}, vectors), and reflectivity at 1.5 km (dBZ, shaded) for 0600 UTC 26 July 2011, and (b) accumulated rainfall amount (mm, shaded) for 0600 UTC 26-0000 UTC 27 July 2011. Results at a grid size of 2.5 km from the FTKP experiment. In (b), solid (for positive values) and dashed lines (for negative values) indicate the difference in the rainfall amount between the CTRL and FTKP experiments (i.e., CTRL-FTKP).

c. Terrain effects on the heavy rainfall

The replacement of the topography of the Korean Peninsula with a flat ground surface in the FTKP simulation did not seriously affect the development of the middle ridge and strong convective systems over the southern coast of HHD at 0600 UTC (Fig. 16a). However, this change resulted in a significant reduction of the 18-h rainfall amount over the middle peninsula compared with the CTRL simulation, especially north and south of Seoul (Fig. 16b). The FTKP significantly over-predicted the rainfall over the east coast area and area the north of GGD. This result indicates that the terrain of the Korean Peninsula contributed to an enhancement of rainfall

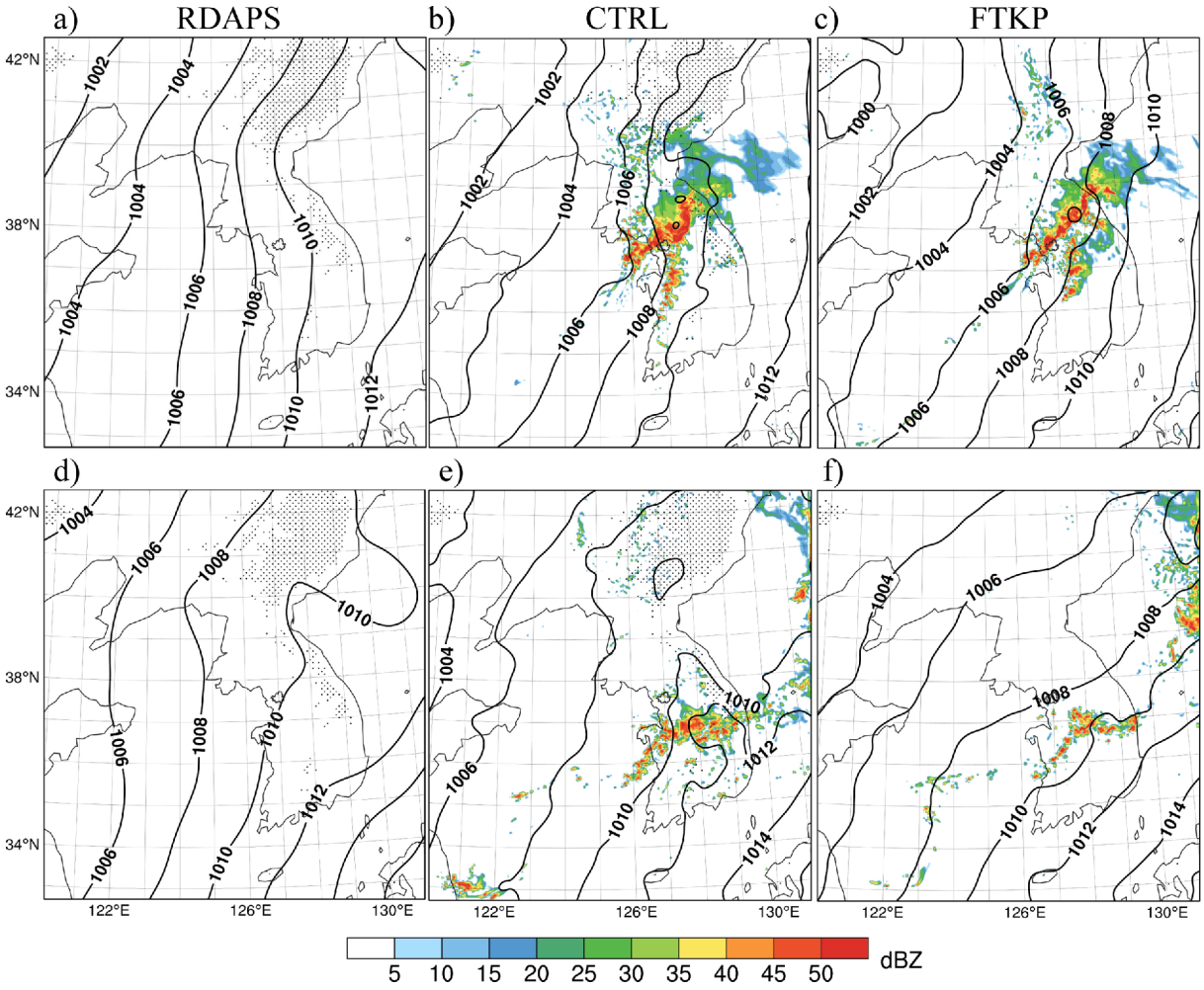

Fig. 17. Sea-level pressure (hPa, solid lines) from the RDAPS (left panels), CTRL (central panels) and FTKP (right panels) experiments for 1200 UTC 26 July (upper panels) and 0000 UTC 27 July 2011 (bottom panels). The simulated reflectivity at 1.5 km from the CTRL and FTKP are also shown. Simulated results are from 2.5-km grid simulations. The stippled area indicates the region with a model terrain height greater than 700 m.

over the middle Korean Peninsula but the suppression of the precipitation to the east of the Taebaek Mountain range. As also found in Fig. 11b, the area-averaged hourly rainfall amount from the FTKP was generally smaller than that from the CTRL simulation, especially during the nighttime.

To explain the terrain effect on the heavy rainfall described above, we examined how the mountainous terrain affected the environment of the HPS development by comparing the results of the CTRL and FTKP simulations. The numerical simulation presented here was limited in the selection of the initial time. It successfully reproduced the initiation of the HPSs at 0600 UTC, only when it was initialized at 0000 UTC 26 July, which was approximately 6 hours before the HPSs formed at 0600 UTC, and initialization at earlier times did not reproduce the HPS development. Because the initial fields at 0000 UTC 26 July may contain terrain effects, it is difficult to isolate the terrain effects in the early stage. Thus, the investigation was focused on the terrain effects on the formation of the northern ridge and the sustained development of heavy rainfall over the west-middle Korean Peninsula during stage 2.

Figure 17 shows the SLP distributions from RDAPS and the two simulations for the 2.5-km grid domain (d03). The results for the general SLP pattern and the quasi-stationary northern ridge from the CTRL simulation were consistent with the RDAPS results. When a flat terrain was assumed over the entire Korean Peninsula in the FTKP simulation, the northern ridge did not appear (Figs. 17c and 17f). Instead, a broad, synoptic-scale trough associated with a cyclone over northern China dominated the Korean Peninsula at 1200 UTC 26 July. A shortwave trough developed along this broad trough in association with convective systems. The control simulation for 0000 UTC 27 July showed a mesoscale ridge and trough upstream and downstream of the Taebaek Mountain range, respectively (Fig. 17e). However, a smoother isobar pattern without a significant ridge was found over the middle part in the FTKP simulation (Fig. 17f). Thus, the Taebaek Mountain

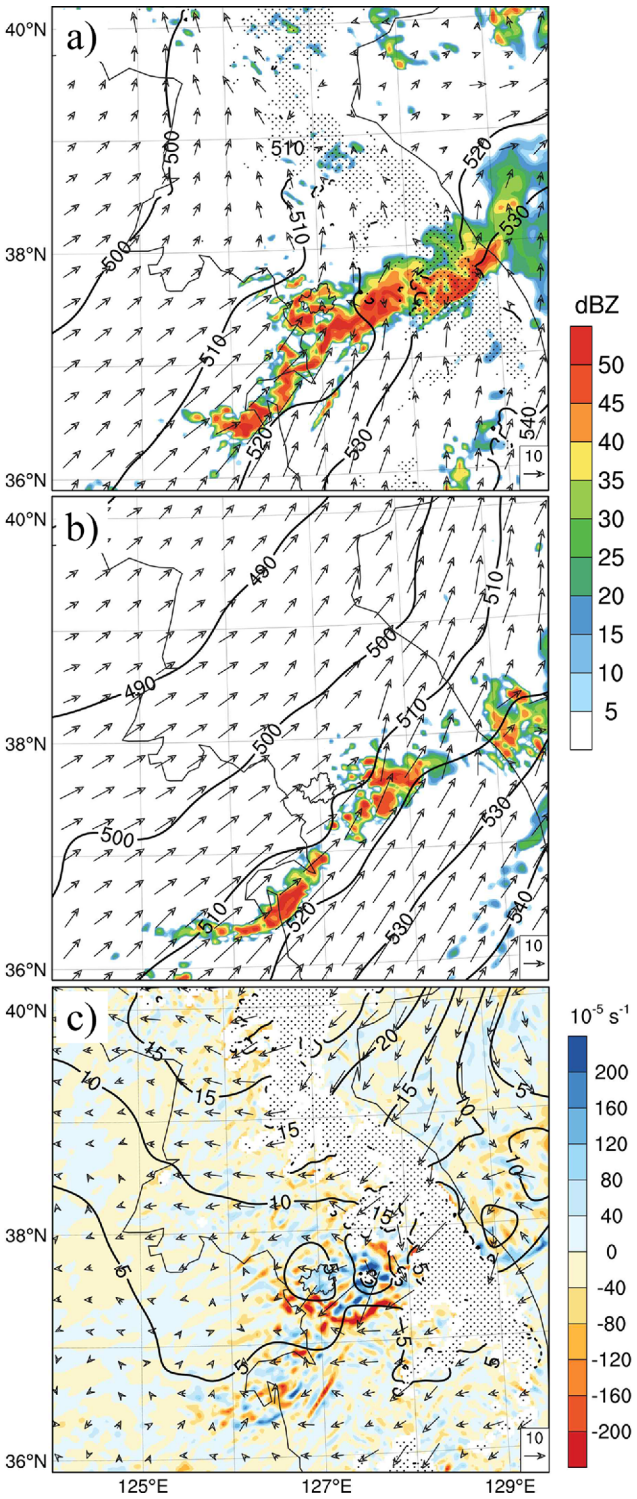

Fig. 18. The geopotential height (m, solid lines) and winds (m s^{-1}, vectors) at 950 hPa and reflectivity at 1.5 km from (a) the CTRL and (b) the FTKP simulation for 1800 UTC 26 July 2011. (c) Differences in the geopotential height (m, solid and dashed lines for positive and negative differences), horizontal divergence (10^{-5} s^{-1}, shaded) and winds (m s^{-1}, vectors) at 950 hPa between the CTRL and FTKP simulations for 1800 UTC 26 July 2011. The stippled areas in (b) and (c) indicate the regions with model terrain height greater than 500 m.

range was also found to significantly affect the adjacent pressure and wind fields.

Figure 18 shows an explanation of the terrain effects on the heavy rainfall. The height and wind fields at 950 hPa for 1800 UTC 26 July from the CTRL and FTKP simulations show significant differences over the peninsula, with mesoscale ridges found throughout the peninsula in the CTRL simulation, which resulted in a weak height gradient over the inland area (Fig. 18a), and height contours found across the peninsula in a SW-NE direction with embedded short waves in the FTKP simulation (Fig. 18b). During stage 2, Froude number (Fr = U/Nh, where U is the speed of wind perpendicular to Taebaek Mountain range, N is the buoyancy oscillation frequency, and h is the terrain height which was assumed as 700 m, respectively) calculated over a box in Fig. 9b was lower than 1 (not shown). In the low Fr regime (Fr < 1), the blocking effect can be significant (Pierrehumbert, 1984; Wang et al., 2005) and windward ridging and leeside troughing can occur (e.g., Smith, 1982; Chen and Li, 1995). Consequently, the CTRL experiment indicated significantly weaker winds over the peninsula than the FTKP experiment because of the blocking effect of the mountains. As a result, a rapid change in wind speed occurred over the mid-western part of the peninsula in the CTRL simulation. Note also that the mesoscale trough over the mid-western part of the peninsula tended to be strong and quasi-stationary because of the presence of a mesoscale ridge upstream of the Taebaek Mountain range in the CTRL simulation, whereas the weak shortwaves traveled northeastward relatively fast in the FTKP simulation. This difference in the mesoscale trough over the mid-western part of the peninsula appears to be important for the larger rainfall amount in the CTRL simulation. Terrain effects can also be demonstrated by showing the differences in height, winds and horizontal divergence at 950 hPa between the CTRL and FTKP simulations (Fig. 18c). Positive height differences were found throughout the peninsula, and the maximum difference was present over the KMC area. The positive differences could also have been caused by the synoptic-scale trough movement toward the east in the FTKP simulation. Differences in the divergence indicate that the convergence over the mid-western part of the peninsula was significantly stronger in the CTRL simulation, although the convergence may have been affected by the convective systems. The above analyses indicate that the terrain of the Korean Peninsula contributed to the enhancement of rainfall amount over the middle peninsula during stage 2 through its blocking effects on the upstream wind fields and the horizontal divergence at low levels over the mid-western part of the peninsula.

Kim and Lee (2006) also found that the terrain of the Korean Peninsula could enhance heavy rainfall over the inland area of the middle Korean Peninsula in a study of a different case, and they also found blocking effects on the movement of the MCSs over the middle Korean Peninsula due to the Taebaek Mountain range.

Heavy rainfalls over the Korean Peninsula are often pro-

duced by cloud cluster type HPSs associated with mesoscale depressions that move toward the Korean Peninsula (Shin and Lee, 2015) or band-type HPSs that often form in between the quasi-stationary large scale flows associated with the WPSH to the south and synoptic-scale low to the north of the peninsula (Lee and Kim, 2007). The present case does not belong to the two types mentioned above in terms of typical synoptic-scale environment and mesoscale disturbances associated with HPSs. It is unique in that cold pool triggers the development of HPSs and plays an important role in sustained heavy rainfalls over the middle Korean Peninsula during stage 1, and that blocking effect of terrain weakens the oncoming southwesterly flow over inland area of the middle peninsula and produces an area of significant horizontal convergence near the west coast in stage 2, resulting in an enhanced heavy rainfall over the Korean Peninsula. Recently, Jeong et al. (2016) studied a case of heavy rainfall caused by a quasi-stationary MCS over southeastern Korea. They found that new convective cells were repeatedly initiated at the leading edge of a cold pool and that the cold pool had an essential role in stationarity of MCS, which resulted in extreme rainfall over Busan metropolitan area. This finding about the role of cold cool is similar to that from the present study, although synoptic-scale pressure pattern and geographical location are different from the present study.

4. Summary and conclusions

In this investigation, an observation analysis and a numerical model were used to explain the heavy rainfall event from 26-27 July 2011 over the middle Korean Peninsula. The heavy rainfall event occurred between a stagnant high-pressure system and a continental low to the east and west of the Korean Peninsula, respectively. These large-scale conditions produced steady and strong south-to-southwesterly flows at low levels over the YS and the west coast of the Korean Peninsula, thereby providing favorable conditions for the development of HPSs over the middle Korean Peninsula. Moreover, a stationary mesoscale ridge (i.e., the northern ridge) extending northwestward from Wonsan persisted at low levels over the northern Korean Peninsula throughout the study period.

Radar observations revealed a significant transition in the echo pattern, with strong convective systems along the coasts of the southern HHD and GGD (0600-1200 UTC 26 July, stage 1); a medium SW-NE band of precipitation over the middle Korean Peninsula and major convective systems in the west (1500-2200 UTC 26 July, stage 2); and a narrow convective band from Gyeonggi Bay to the Seoul metropolitan area (2200 UTC 26-0100 UTC 27 July, stage 3). This investigation focused on the development of the HPSs during stages 1 and 2.

A well-defined mesoscale ridge (i.e., the middle ridge) and trough pair developed over the middle Korean Peninsula at approximately 0600 UTC 26 July, with strong convective systems along the southern side of the ridge. The observational analysis indicated that the middle ridge and trough pair developed as the ridge formed in response to the cooling of low-level air. The cooling was related to the evaporation of rain water. The ridge played an important role in the continuous development of strong convective systems over the middle Korean Peninsula during stage 1. The convergence of the low-level flows along the southern side of the ridge might have been the major triggering mechanism for the strong convective systems in stage 1. This convergence occurred as a surface easterly flow developed along the southern side of the ridge in the presence of prevailing surface southerly or southwesterly winds over the sea (i.e., to the south of the ridge).

During stage 2, major convective systems developed over the western part of the precipitation band, and the middle ridge and trough pair persisted over the middle Korean Peninsula. The lifting of air for these convective systems was mainly caused by the convergence ahead of the strong southwesterly flow below 800 hPa.

Numerical experiments were performed to examine the formation processes of the northern and middle ridges and the effect of the mountainous terrain on the environment of the HPS development. The control simulation successfully reproduced the major features of the HPS patterns and their associated meteorological fields, including the middle ridge and trough pair over the middle Korean Peninsula during 0600-1200 UTC 26 July. The simulation showed that a surface easterly developed along the southern side of the middle ridge and low-level convergence between the easterly and southerly airflow from the sea provided the lift for low-level air beyond the LFC at 0600 UTC. However, the simulated HPSs and the amount of rainfall after 1200 UTC were significantly different from the observations and failed to replicate the observed narrow convective band in stage 3.

The control and sensitivity simulations showed that the middle ridge and trough pair developed as the ridge formed in response to the evaporative cooling of the low-level air during a decrease in SLP over the Korean Peninsula. The surface easterly flow along the southern side of the middle ridge was mainly caused by the development of an outflow associated with a cold pool over inland HHD. In addition, the land-sea contrast of surface friction was not important for the triggering mechanism of the convective development along the coast.

The mountainous terrain over the Korean Peninsula was found to enhance the heavy rainfall over the middle Korean Peninsula, primarily by modifying the environment. (1) The KMC contributed to the maintenance of N-S oriented isobars along the west coast of the north-to-middle Korean Peninsula by inducing the formation of the northern ridge, (2) The blocking effects of the Taebaek Mountain range and KMC at night produced an area with a weak pressure gradient over the middle Korean Peninsula. These effects may have contributed to the sustained development of HPSs over the middle Korean Peninsula, and the latter effect might have contributed to the horizontal convergence ahead of a strong southwesterly flow in the lower troposphere over the west-middle Korean Peninsula, where the southwesterly flow from the YS rapidly weakened as it moved inland. The environmental convergence

ahead of the strong southwesterly flow in a potentially unstable condition may have created a favorable environment for inland-moving convective cells to grow into deep systems. The present study indicates that forecast of heavy rainfall over the middle Korean Peninsula, in a synoptic condition similar to the present case, may need to consider the effect of the terrain over the Korean Peninsula. In this study, the roles of Taebaek Mountain range and KMC are not discussed separately. Further study is needed to understand their roles in the heavy rainfall over the middle Korean Peninsula.

Acknowledgements. This work was funded by the Korea Meteorological Administration Research and Development Program under Grant KMIPA 2015-5080. The authors thank editor and three anonymous reviewers for their valuable comments and suggestions during the review process.

Edited by: John Richard Gyakum

References

Bluestein, H. B., and M. H. Jain, 1985: Formation of mesoscale lines of precipitation: severe squall lines in Oklahoma during the spring. *J. Atmos. Sci.*, **42**, 1711-1732, doi:10.1175/1520-0469(1985)042<1711:FOMLOP>2.0.CO;2.

Chen, C.-S., W.-S. Chen, and Z. Deng, 1991: A study of a mountain-generated precipitation system in Northern Taiwan during TAMEX IOP 8. *Mon. Wea. Rev.*, **119**, 2574-2607, doi:10.1175/1520-0493(1991)119<2574:ASOAMG>2.0.CO;2.

Chen, Y.-L., and J. Li, 1995: Characteristics of surface air-flow and pressure patterns over the island of Taiwan during Tamex. *Mon. Wea. Rev.*, **123**, 695-716, doi:10.1175/1520-0493(1995)123<0695:COSAAP>2.0.CO;2.

Choi, H.-Y., J.-H. Ha, D.-K. Lee, and Y.-H. Kuo, 2011: Analysis and simulation of mesoscale convective systems accompanying heavy rainfall: the Goyang case. *Asia-Pac. J. Atmos. Sci.*, **47**, 265-279, doi:10.1007/s13143-011-0015-x.

Hong, S.-Y., 2004: Comparison of heavy rainfall mechanisms in Korea and the central US. *J. Meteor. Soc. Japan*, **82**, 1469-1479, doi:10.2151/jmsj.2004.1469.

_____, and J.-O. J. Lim, 2006: The WRF single-moment 6-class microphysics scheme (WSM6). *J. Korean Meteor. Soc.*, **42**, 129-151.

Iacono, M. J., J. S. Delamere, E. J. Mlawer, M. W. Shephard, S. A. Clough, and W. D. Collins, 2008: Radiative forcing by long-lived greenhouse gases: calculations with the AER radiative transfer models. *J. Geophys. Res.*, **113**, D13103, doi:10.1029/2008JD009944.

Janjić, Z. I., 1994: The step-mountain eta coordinate model: Further developments of the convection, viscous sublayer, and turbulence closure schemes. *Mon. Wea. Rev.*, **122**, 927-945, doi:10.1175/1520-0493(1994)122<0927:TSMECM>2.0.CO;2.

Jeong, J.-H., D.-I. Lee, and C.-C. Wang, 2016: Impact of Cold Pool on Mesoscale Convective System Produced Extreme Rainfall over southeastern South Korea: 7 July 2009. *Mon. Wea. Rev.*, **144**, 3985-4006, doi:10.1175/MWR-D-16-0131.1.

Kain, J. S., 2004: The Kain-Fritsch convective parameterization: An update. *J. Appl. Meteorol.*, **43**, 170-181, doi:10.1175/1520-0450(2004)043<0170:TKCPAU>2.0.CO;2.

Kato, T., 1998: Numerical simulation of the band-shaped torrential rain observed over southern Kyushu, Japan on 1 August 1993. *J. Meteor. Soc. Japan*, **76**, 97-128.

Kim, D.-K., and H.-Y. Chun, 2000: A numerical study of the orographic effects associated with a heavy rainfall event. *J. Korean Meteor. Soc.*, **36**, 441-454 (in Korean with English abstract).

Kim, H. W., and D. K. Lee, 2006: An observational study of mesoscale convective systems with heavy rainfall over the Korean Peninsula. *Wea. Forecasting*, **21**, 125-148, doi:10.1175/WAF912.1.

KMA, 2012: Learning from the cases in recent 20 years - top ten heavy rainfall events. Korea Meteorological Administration, Seoul, 47 pp (in Korean).

Lee, D.-K., J.-G. Park, and J.-W. Kim, 2008: Heavy rainfall events lasting 18 days from July 31 to August 17, 1998, over Korea. *J. Meteor. Soc. Japan*, **86**, 313-333, doi:10.2151/jmsj.86.313.

Lee, J.-T., D.-I. Lee, C.-H. You, H. Uyeda, Y.-C. Liou, and I.-S. Han, 2014a: Dual-Doppler radar analysis of a near-shore line-shaped convective system on 27 July 2011, Korea: a case study. *Tellus*, **66**, 23453, doi:10.3402/tellusa.v66.23453.

Lee, J. G., and Y. J. Kim, 2009: A numerical case study examining the orographic effect of the northern mountain complex on snowfall distribution over the Yeongdong region. *Atmosphere*, **19**, 345-370 (in Korean with English abstract).

Lee, K.-O., H. Uyeda, and D.-I. Lee, 2014b: Effect of an isolated elliptical terrain (Jeju Island) on rainfall enhancement in a moist environment. *Tellus*, **66**, 20484, doi:10.3402/tellusa.v66.20484.

Lee, T.-Y., and Y.-Y. Park, 1996: Formation of a mesoscale trough over the Korean peninsula during an excursion of the Siberian High. *J. Meteor. Soc. Japan*, **74**, 299-323.

_____, and Y.-H. Kim, 2007: Heavy precipitation systems over the Korean peninsula and their classification. *J. Korean Meteor. Soc.*, **43**, 367-396.

_____, Y.-Y. Park, and Y.-H. Kim, 1998a: A numerical modeling study of heavy rainfall development over the Changma front. *Proc., International Conference on Monsoon and Hydrologic Cycle*, Kyongju, Korea, 72-75.

_____, _____, and Y.-L. Lin, 1998b: A numerical modeling study of mesoscale cyclogenesis to the east of the Korean peninsula. *Mon. Wea. Rev.*, **126**, 2305-2329, doi:10.1175/1520-0493(1998)126<2305:ANMSOM>2.0.CO;2.

Lim, E.-H., and T.-Y. Lee, 1994: Two-dimensional numerical study of the terrain effects on the development of cloud and precipitation for the middle part of Korea. *J. Korean Meteoro. Soc.*, **30**, 565-582 (in Korean with English abstract).

Nagata, M., 1991: Further numerical study on the formation of the convergent cloud band over the Japan Sea in winter. *J. Meteor. Soc. Japan*, **69**, 419-428.

NEMA, 2012: Annual disaster report for 2011. National Emergency Management Agency, Seoul, 973 pp (in Korean).

Pierrehumbert, R. T., 1984: Linear results on the barrier effects of mesoscale mountains. *J. Atmos. Sci.*, **41**, 1356-1367, doi:10.1175/1520-0469(1984)041<1356:LROTBE>2.0.CO;2.

Saha, S., and Coauthors, 2010: The NCEP climate forecast system reanalysis. *Bull. Amer. Meteor. Soc.*, **91**, 1015-1057, doi:10.1175/2010BAMS3001.1.

Seo, K.-H., and D.-K. Lee, 1996: Analysis and simulation of orographic rain in the middle part of the Korean Peninsula. *Asia-Pac. J. Atmos. Sci.*, **32**, 511-533 (in Korean with English abstract).

Shin, C.-S., and T.-Y. Lee, 2005: Development mechanisms for the heavy rainfalls of 6-7 August 2002 over the middle of the Korean Peninsula. *J. Meteor. Soc. Japan*, **83**, 683-709, doi:10.2151/jmsj.83.683.

Shin, U., and T.-Y. Lee, 2015: Origin, evolution and structure of meso-alpha-scale lows associated with cloud clusters and heavy rainfall over the Korean peninsula. *Asia-Pac. J. Atmos. Sci.*, **51**, 259-274, doi:10.1007/s13143-015-0076-3.

Skamarock, W. C., J. B. Klemp, J. Dudhia, D. O. Gill, D. M. Barker, M. G.

Duda, X. Y. Huang, W. Wang, and J. G. Powers, 2008: A description of the advanced research WRF V.3. NCAR Tech. Note NCAR/TN-475+STR, 113 pp.

Smith, R. B., 1982: Synoptic observations and theory of orographically disturbed wind and pressure. *J. Atmos. Sci.*, **39**, 60-70, doi:10.1175/1520-0469(1982)039<0060:SOATOO>2.0.CO;2.

Tsuguti, H., and T. Kato, 2014: Contributing factors of the heavy rainfall event at Amami-Oshima Island, Japan, on 20 October 2010. *J. Meteor. Soc. Japan*, **92**, 163-183, doi:10.2151/jmsj.2014-202.

Wang, C.-C., G. T.-J. Chen, T.-C. Chen, and K. Tsuboki, 2005: A numerical study on the effects of Taiwan topography on a convective line during the mei-yu season. *Mon. Wea. Rev.*, **133**, 3217-3242, doi:10.1175/MWR3028.1.

Yamada, H., B. Geng, K. K. Reddy, H. Uyeda, and Y. Fujiyoshi, 2003: Three-dimensional structure of a mesoscale convective system in a Baiu-frontal depression generated in the downstream region of the Yangtze river. *J. Meteor. Soc. Japan*, **81**, 1243-1271, doi:10.2151/jmsj.81.1243.

Yoshizaki, M., T. Kato, Y. Tanaka, H. Takayama, Y. Shoji, H. Seko, K. Arao, and K. Manabe, 2000: Analytical and numerical study of the 26 June 1998 orographic rainband observed in western Kyushu, Japan. *J. Meteor. Soc. Japan*, **78**, 835-856.

Zhang, Y., L. F. Zhang, C. M. Wang, Y. Q. Xie, and J. Xiang, 2014: Mechanism of a torrential rainstorm that occurred to the west of a Mei-yu frontal low. *Asia-Pac. J. Atmos. Sci.*, **50**, 437-452, doi:10.1007/s13143-014-0034-5.